Non-coalescence of Jets

Navish Wadhwa

Thesis submitted to the faculty of the Virginia Polytechnic Institute and State University
in partial fulfillment of the requirements for the degree of

Master of Science
In
Engineering Mechanics

Sunghwan Jung, Committee Chair

Pavlos P. Vlachos

John J. Socha

April 30, 2012
Blacksburg, VA

Keywords: Non-coalescence, bouncing jets, contact time, transition

Non-coalescence of Jets

Navish Wadhwa

Abstract

Contrary to common intuition, free jets of fluid can ``bounce'' off each other on collision in mid-air, through the effect of a lubricating air film that separates the jets. While there has been much work on coalescing jets of fluid and non-coalescence in other systems like drop-drop, drop on a bath, jet on a bath, non-coalescence of fluid jets has been little studied. A simple experimental setup was developed to stably demonstrate and study the non-coalescence of jets upon collision. This thesis presents the results of an experimental investigation of oblique collision between two fluid jets. The transition from bouncing to coalescence of jets is examined for various jet sizes and angles. Results indicate that the transition from bouncing to coalescence can be rationalized in terms of critical value of the dimensionless parameter Normal Weber Number, which represents the ratio between inertial and surface tension forces. A parametric study of the characteristic of bouncing jets, conducted by varying the nozzle diameter, jet velocity, angle of inclination and fluid viscosity reveals the scaling laws for the quantities involved such as contact time. These scaling laws help us in elucidating the role of various physical forces at play such as viscous stresses, capillary force and inertia.

For my parents…

Acknowledgements

A huge credit for this work goes to Dr. Sunghwan Jung, for much of the ideas and insight required for this work came from him. I thank him not only for painstakingly guiding me through this work over the last two years, but also for the unfaltering support I received from him on multiple fronts.

Dr. Pavlos Vlachos played a very important role in the development of this work. Some of defining ideas for this work came through the discussions with him or while trying to answer the questions put forward by him.

Dr. Jake Socha gave very useful inputs which helped a lot in improving the quality of this work. I also thank him for being a great teacher and mentor. Over the last year in which I have interacted with him, he has always given me some of the most useful advice and feedback on various issues ranging from communication of ideas to approach towards science.

I would also like to thank Dr. Shane Ross, Dr. Douglas Holmes, Dr. Anne Ryan and Liaosa Xu for useful discussion during this work. I also want to thank my previous advisors, Dr. Sanjay Sane and Dr. Brijesh Eshpuniyani, for they made me the researcher I am today and had a tremendous influence on the way I do science.

I want to thank all member of the Bio-Inspired Fluids Lab, particularly Saikat Jana, Sean Gart, Daniel Chique and Brian Chang, for providing me with such a lively and fun environment to work in. For good times and companionship, I thank Nikhil Jain, Sudarshan Gopinath, Pallavi Bishnoi, Shalini Ramesh, Natasha Das, Hiba Assi, Vireshwar Kumar, Prabuddha Bansal and Omid Ghasemalizadeh. And to my close friends elsewhere in US and around the world, Maria Masoodi, Arun Garg, C Ashish Kumar, Vardhman Jain, Othy Shivashankar, Guncha Dwivedi, thanks for staying in touch despite the distance.

Finally, special thanks to my family for being the staunch supporters throughout my life, for encouragement to pursue my dreams and for being with me through the worst of my times. To my father, Vinod Kumar and my mother, Preeti Wadhwa, I cannot thank you

enough for everything that you have done for me. I am forever indebted to you for all I have in life now and for all that I may have in the future.

Table of contents

Abstract ii
Acknowledgements iv
Table of contents vi
List of Figures viii
Chapter 1: Introduction 1
1.1 Bouncing Jets 1
1.2 Conditions for bouncing 6
1.3 Contact time of the jets 6
1.3 Overview of the thesis 8
Chapter 2: Background and Literature 9
2.1 Bouncing jets 9
2.2 Drops bouncing on a stationary free surface of fluid 10
2.3 Drops bouncing on an oscillating free surface of fluid 11
2.4 Jet bouncing on free surface of fluid 13
2.5 Drops bouncing on hydrophobic surface 14
2.6 Colliding drops 15
2.7 Colliding bubbles 16
2.8 Drops bouncing on soap film 16
Chapter 3: Methods and Materials 18
3.1 Experimental Setup 18
3.2 Experimental Procedures and Imaging 20
3.3 Image Analysis 23
Chapter 4: Results and discussion 25
4.1 Transition from non-coalescence to coalescence 25
4.2 Contact time of bouncing jets 36
Chapter 5: Conclusions 48
5.1 Transition from bouncing to coalescence 48
5.2 Contact time of bouncing jets 48
5.3 Summary 49
5.4 Suggestions for future work 49
References 51

Appendix A: MATLAB© code for image analysis 55

List of Figures

Figure 1: Two silicone oil (ν = 10 cSt) jets of diameter approximately 500 μm collide obliquely and bounce from each other. 2

Figure 2: Two side jets bounce off a middle jet. The collision causes instability in the middle jet resulting in its break into droplets. See [1]. 3

Figure 3: Three silicone oil jets collide obliquely with each other. The jets do not coalesce upon collision and bounce off into three different directions. 4

Figure 4: Series of drops from two sides collide with a jet without merging into it. The collision with drops causes the jet to bend in two locations. 5

Figure 5: Schematic showing how the collision between the jets can be seen as two dimensional droplets moving with the jets. Top: Side view of the jets showing the cross-section of the jets as it moves down with them. Bottom: Top view of the corresponding cross-section, appearing as two drops colliding with each other. 7

Figure 6: Two water jets dyed with different colors bounce after colliding with each other. The jets retain their colors after the collision showing that there is no material transport between the jets upon collision. 10

Figure 7: Levitation of a water drop on a hydraulic jump is shown in inclined view (top) and side view (bottom). The numbers in the images are the volume of the drop. The hydraulic jump was created by a vertical water jet hitting a glass plate at about 8 cms^{-1}.. 11

Figure 8: A series of images showing a droplet bouncing over an oscillating fluid bath moves due to interaction with its own wave field generated on the surface..... 13

Figure 9: A Newtonian fluid jet bouncing off the surface of a moving bath of same fluid. 14

Figure 10: Experimental setup. Two 3 axis translation stages are used for precise positioning of the needles. A syringe pump pushes fluid through two identical needles to form jets. The fluid is collected in a glass beaker after collision. 19

Figure 11: Typical image of bouncing jets showing the quantities of interest; α is the angle between the jet and the vertical axis and *l* is the length of contact region of the bouncing jets 22

Figure 12: Snapshot of the image analysis code output. Midpoint between points 1 and 2 gives the point where the collision starts, while midpoint between points 3 and 4 is the point where the jets separate. 24

Figure 13: Series of images show the re-initiation of bouncing by perturbation of two coalesced jets using a needle..... 26

Figure 14: Bouncing life-time versus jet velocity for different jet angles in Gauge 16 experiments. Points denote the median life-time of bouncing while the error bars are of length equal to half of MAD on each side. Red arrows indicate transition velocity. 27

Figure 15: Transition velocity versus jet angle α for Gauge 16. The critical velocity required for coalescence decreases as α increases. 29

Figure 16: Transition velocity versus jet angle α for Gauge 18. The critical velocity required for coalescence decreases as α increases. 30

Figure 17: Transition velocity versus jet angle α for Gauge 19. As seen in the transition curves for other needle sizes, the transition velocity decreases as α increases. 31

Figure 18: Transition velocity versus jet angle α for Gauges 16, 18 and 19. The transition curves for different needle sizes shows similar trends and lie almost parallel to each other. 32

Figure 19: Characteristic length scale used to define the Normal Weber Number $We_{\perp}$.. 33

Figure 20: Normal Weber Number $We_{\perp}$ versus jet angle α for Gauge 16 (circles), 18 (triangles) and 19 (diamonds). Black markers represent bouncing and red markers represent coalescence cases. Horizontal line represents the critical Normal Weber Number $We_{\perp}^{*}$ = 8.23, at which the transition from bouncing to coalescence takes place. 34

Figure 21: Transition velocity versus jet angle α for Gauges 16, 18 and 19. Solid lines represent experimentally determined transition velocities and dashed lines represent those calculated from critical Normal Weber Number $We_{\perp}^{*}$= 8.23. 35

Figure 22: Scatter plot of dimensionless contact time ($T_{contact}^{*}$) against Normal Weber Number (We) for ν = 10 cSt. Size of dots correlates with the size of jets, but there is no quantitative relationship between the sizes. 38

Figure 23: Scatter plot of dimensionless contact time ($T_{contact}^{*}$) against Normal Weber Number (We) for ν = 50 cSt. 39

Figure 24: Scatter plot of dimensionless contact time ($T_{contact}^{*}$) against Normal Reynolds Number (Re) for ν = 10 cSt. 40

Figure 25: Scatter plot of dimensionless contact time ($T_{contact}^{*}$) against Normal Reynolds Number (Re) for ν = 50 cSt. 40

Figure 26: Scatter plot of dimensionless contact time ($T_{contact}^{*}$) against Normal Reynolds Number (Re) for ν = 10 cSt (black dots) and ν = 50 cSt (blue dots). 42

Figure 27: Scatter plot of dimensionless contact time ($T_{contact}^{*}$) against Normal Weber Number (We) for ν = 10 cSt (black) and ν = 50 cSt (blue). 43

Figure 28: Logarithmic plot between dimensionless contact time ($T_{contact}^{*}$) against Normal Weber Number (We) for ν = 10 cSt (black) and ν = 50 cSt (blue). Straight line is

the best fit line on the data with slope = 0.467, confidence bounds = (0.4336, 0.4997), R^2 = 0.85. 44

Figure 29: Logarithmic plot between dimensionless contact time ($T^*_{contact}$) against Normal Weber Number (We) for ν = 10 cSt (black), ν = 50 cSt (blue) and 75% by weight glycerol solution. Straight line is the best fit line on the data with slope = 0.462, confidence bounds = (0.4302, 0.4942), R^2 = 0.85. 45

Figure 30: $\frac{T_{contact}}{\sin\alpha}$ verses the jet velocity *V*. Data points for different jet sizes are denoted by different colors and show no trend with change in the jet velocity. 46

Figure 31: Logarithmic plot between $\frac{\mathrm{T_{contact}}}{\sin\alpha}$ and the jet diameter *D*. Straight line is the best fit line on the data with slope = 1.53, 95% confidence bounds = (1.32, 1.74), R^2 = 0.99. Error bar is equal one standard deviation long on each side..... 47

Chapter 1: Introduction

1.1 Bouncing Jets

Our day to day experience and intuition tell us that when two streams of fluid are brought together, they readily merge into one stream. Be it dish soap and water mixing to form soap solution or flavored syrup and carbonated water mixing to form fountain soda, fluids always mix together when brought into contact. It is hard to imagine a situation in which one stream of fluid collides with another and instead of merging into it, bounces right off its surface. The thought of that happening almost makes us uncomfortable because it is so counter-intuitive.

Contrary to the expectation, two colliding jets of fluid can actually bounce off without merging into each other in certain situations. Figure 1 shows an image of two jets of silicone oil colliding obliquely with each other and bouncing off after the collision, without coalescing. The diameter of the colliding jets is about 500 μm.

Even though it appears this way to the naked eye, the two jets do not actually come into contact upon collision. They remain separated by a thin film of air, which keeps the two jets apart and prevents coalescence. As the two jets move through the surrounding medium, which is air in this case, they drag it along with them as a result of the no slip boundary condition at the surface. This air gets dragged into the collision region, where it is squeezed into a thin film. This squeezing of air film produces resistive forces high enough to keep the jets apart, much like the lubricating action of oil in a journal bearing.

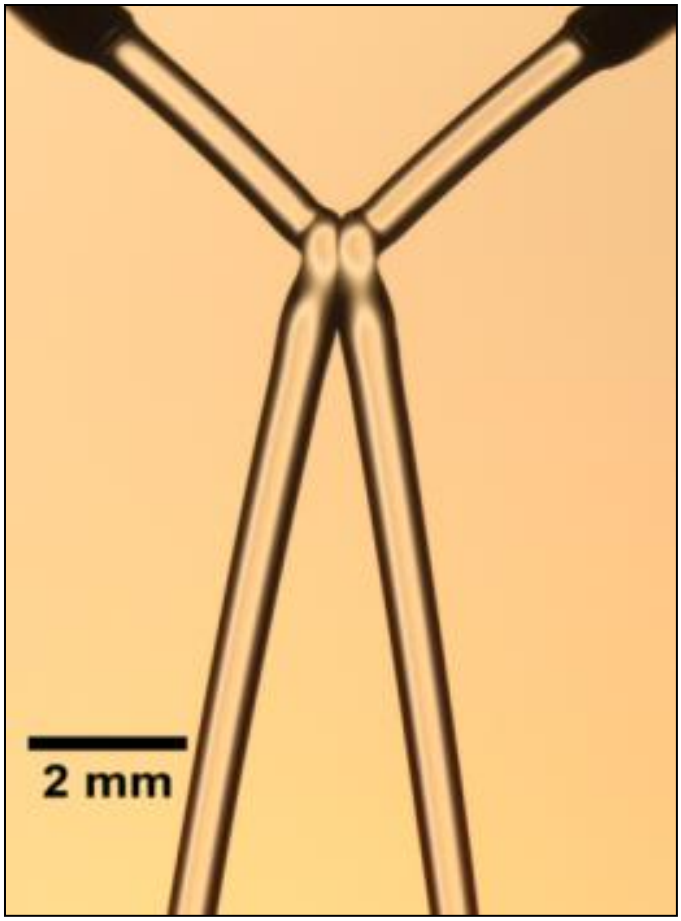

Figure 1: Two silicone oil (ν = 10 cSt) jets of diameter approximately 500 μm collide obliquely and bounce from each other.

It is not just two colliding jets that bounce off each other after the collision. Figure 2 shows three jets in the same vertical plane colliding with each other, with one jet coming vertically downwards and two jets from the two sides. As can be seen in Figure 2, the three jets do not coalesce upon collision. There is a high amount of deformation in the middle jet due to the two jets hitting from the sides, suggesting that high magnitude of forces are involved in the collision, but the jets still do not coalesce. The instability caused by the collision in the middle jet results in the breakup of the middle jet into droplets.

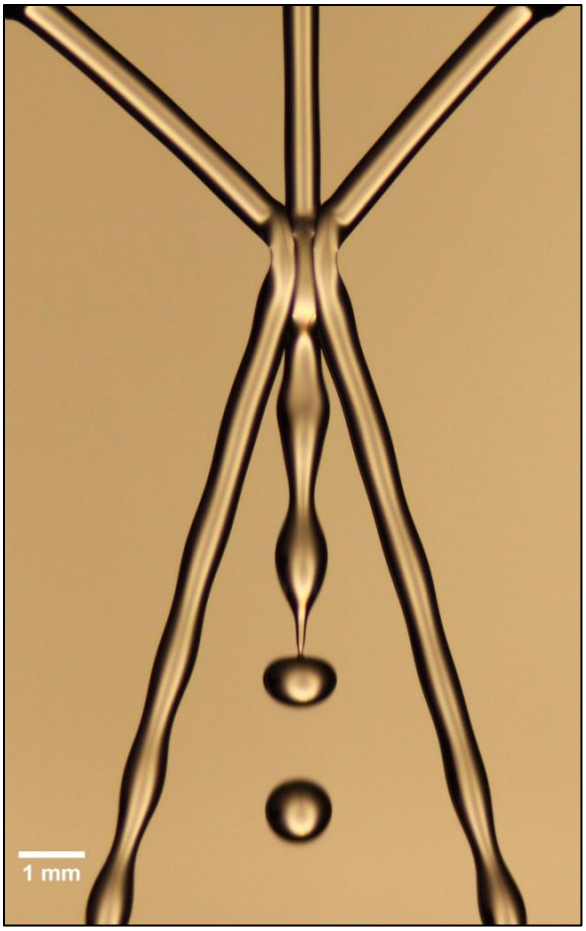

Figure 2: Two side jets bounce off a middle jet. The collision causes instability in the middle jet resulting in its break into droplets. See [1].

The robustness of this non-coalescence behavior in silicone oil jets is demonstrated by the fact that even when multiple colliding jets are not in the same vertical plane, they can bounce off upon collision. Figure 3 shows three silicone oil jets colliding with each other obliquely from three different directions and then bouncing off each other.

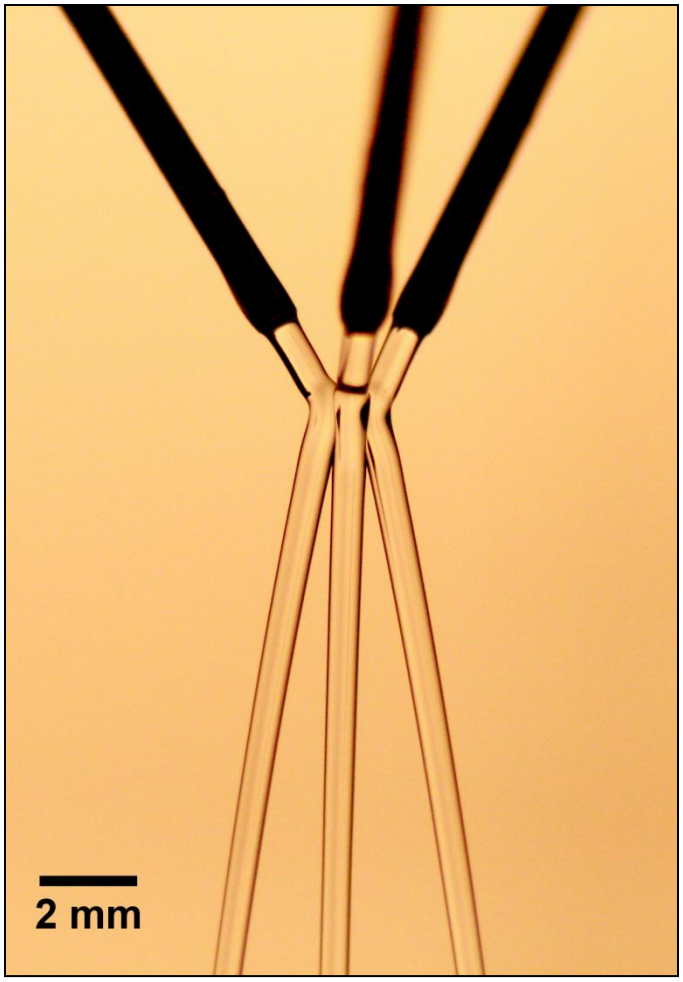

Figure 3: Three silicone oil jets collide obliquely with each other. The jets do not coalesce upon collision and bounce off into three different directions.

It is also possible to observe non-coalescence between a fluid jets and droplets of the same fluid. In one of the experiments with three jets in the same vertical plane, the side jets broke up into droplets when the syringe supplying the two side jets ran out of fluid. Images of collision between the droplets thus formed and the continuous middle jet revealed non-coalescence between fluid drops and jet, as seen in Figure 4. The droplets colliding with the middle jet from two different sides caused it to deform at two locations, without resulting in coalescence.

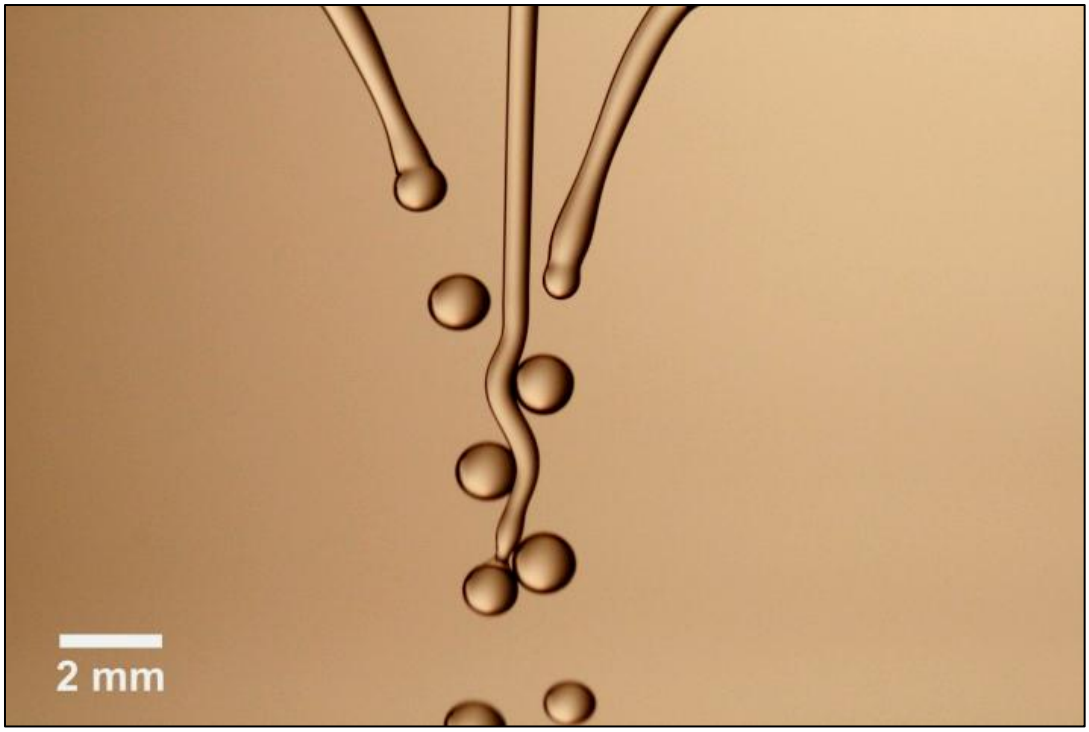

Figure 4: Series of drops from two sides collide with a jet without merging into it. The collision with drops causes the jet to bend in two locations.

This thesis is aimed at illuminating this curious phenomenon and investigating the physical mechanisms responsible for this surprising behavior that defies our intuition.

1.2 Conditions for bouncing

The incoming jets drag along a thin layer of air due to the no slip boundary condition at the surface of the jets. This layer of air gets squeezed into the collision region between the two jets and separates the two jets from each other. Due to the thin gap between the two jets in collision region, the lubrication approximation is applicable to the air film. Because the thickness of the air-film is significantly smaller than the other dimensions, extremely high shear rates are generated and thus the air film is able to generate forces high enough to keep the jets separated from each other.

As can be expected, two colliding jets won't always bounce from each other. Imagine an experiment in which jet size and angle are fixed, and we slowly increase the jet velocity. At small jet velocity, the jets will bounce from each other as it is easier for the separating air-film to counter the small momentum of the incoming jets. But at large velocities, the jets are expected to coalesce, as the air-film will no longer be able to generate the large forces required to keep the jets separated. Thus, there must be a critical jet velocity for this experiment, at which the air-film is in a critical condition and is able to produce forces just high enough to keep the jets apart. This critical velocity is termed as the transition velocity, at which the transition from bouncing of the two jets to coalescence takes place. A central goal of this work is to experimentally investigate the nature of this transition from bouncing to coalescence, for different jet angles and sizes.

1.3 Contact time of the jets

Consider a planar cross-section of the colliding jets in the horizontal plane, as shown in Figure 5. The top frame of Figure 5 shows the side view of the colliding jets and the

bottom frame shows the top view of the cross-section under consideration. Such a cross-section is essentially a two dimensional droplet moving along with the jet with the jet velocity V. As the droplets moves along the jet, in the plane attached to the droplets, it seems as if the droplets encounter a head on collision, as shown graphically in Figure 5. Due to the no slip condition, surrounding air gets dragged along in the same plane and that allows us to view the collision simply as a collision between two dimensional droplets moving through air.

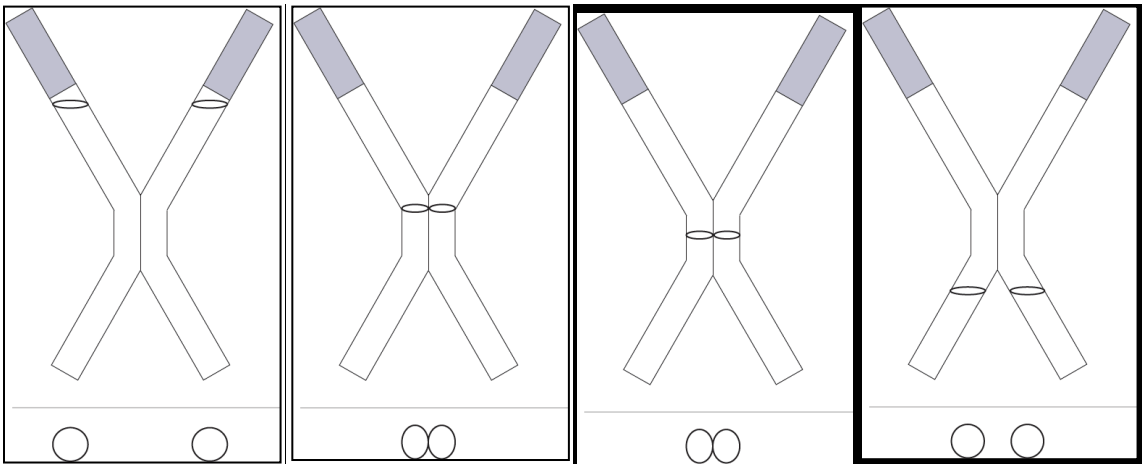

Figure 5: Schematic showing how the collision between the jets can be seen as two dimensional droplets moving with the jets. Top: Side view of the jets showing the cross-section of the jets as it moves down with them. Bottom: Top view of the corresponding cross-section, appearing as two drops colliding with each other.

There is a time scale associated with the rebound of the colliding droplets. This is the time that is spent before the droplets lose the momentum with which they arrive in the collision region and start to bounce back. This time scale has been termed as the *contact time* of the jets/droplets.

By studying the effect of Normal Weber number and Normal Reynolds number on bouncing jets, relative importance of surface tension and viscous forces in the phenomenon of bouncing jets can be understood. The true scaling law for the dimensionless contact time needs to be verified from the experimental results.

1.3 Overview of the thesis

Chapter 1 introduces the phenomenon and proposes a hypothesis for explaining the phenomenon of bouncing jets. Chapter 2 gives an introduction to the past work in this and related areas of investigation. Chapter 3 describes the experimental setup and the methodologies used in the course of this research. Chapter 4 discusses the main results of the investigation and the implications of those results for the understanding of bouncing jets. Chapter 5 summarizes the understanding gained through this work and provides suggestions for future investigations.

Chapter 2: Background and Literature

2.1 Bouncing jets

Lord Rayleigh was the first to observe the curious phenomenon of water drops and jets bouncing off each other [3]. He hypothesized that collision and bouncing of droplets as a cause of normal scattering of droplets formed from an almost vertical jet of water, and also observed the effect of electricity on the normal scattering, relating it to the bouncing of droplets. In his classic paper, he studied the role of electric potential in determining the fate of two jets colliding with each other [3]. He noted that the presence of even a small amount of electric potential difference between the two jets resulted in coalescence between two bouncing jets. In his subsequent papers following up on this, he studied the role of dust and the intervening gas on the non-coalescence between jets [4, 5].

Newall revisited Lord Rayleigh's experiments on water jets and described the colored bands formed in the collision area [6]. By observing the bands under the influence of electricity, he concluded that electric potential had no effect on the thickness of air film between the two jets.

Boys, in his famous book, demonstrated the phenomenon of bouncing jets for juvenile audiences and also explained the role of electricity on the non-coalescence by using a piece of -charged sealing-wax [7]. Figure 6 shows an image from Boys' book, demonstrating how water jets dyed with different colors bounce from each other upon collision and that there is no material transfer from one jet to the other during collision, as the colors of the two jets remain intact.

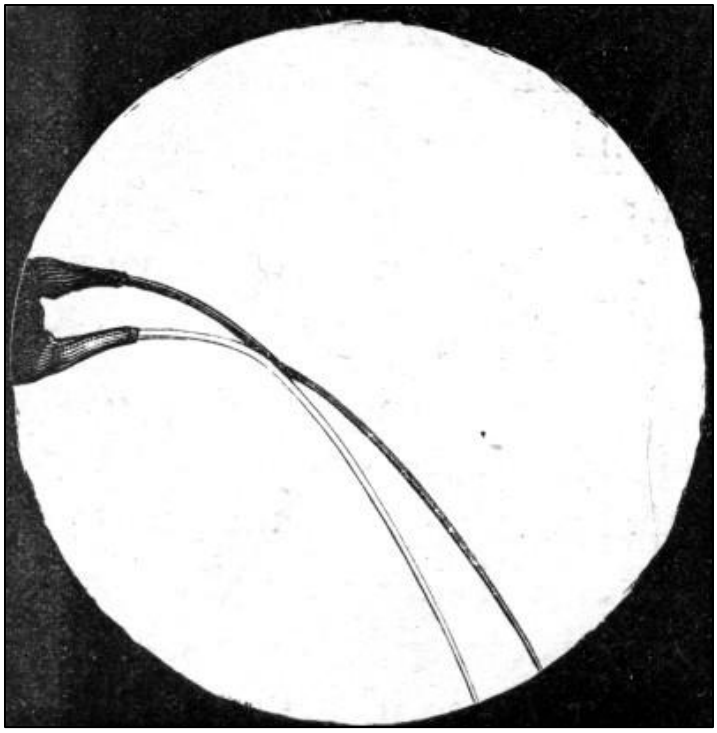

Figure 6: Two water jets dyed with different colors bounce after colliding with each other. The jets retain their colors after the collision showing that there is no material transport between the jets upon collision. Taken from [7] (public domain).

2.2 Drops bouncing on a stationary free surface of fluid

While the non-coalescence of jets remained largely unexplored after the work done by Rayleigh, Newall and Boys, the related phenomenon of bouncing of drops on free surface started gaining attention. Reynolds had reported the floating of drops on free surface of water and concluded that the purity of the surface of water was the primary condition for the drops to float on surface [8]. Seth et al. and Mahajan carried out the first detailed investigation of drops bouncing and studied the effect of fluid viscosity, surface tension, temperature and the surrounding medium on the bouncing behavior [9-11]. They managed to get floating drops as large as 12 mm in diameter and drops which bounced for as long as 5 minutes [9]. They also found that mobile drops are more stable than

stationary drops and that drops formed over a moving stream are more stable. These observations were later confirmed by Sreenivas et al., who reported levitation of fairly large drops just upstream of a hydraulic jump, supported on the air flow maintained by the flow of fluid below [12]. In a pair of papers, Charles and Mason studied the phenomenon of partial coalescence between a drop and a fluid interface and formulated a theory for film thinning and deformation in the drop as it approaches a fluid interface [2, 13]. They carried out high speed photographic measurements of partial and complete coalescence and measured the "rest time" of drop on the interface, which followed their prediction.

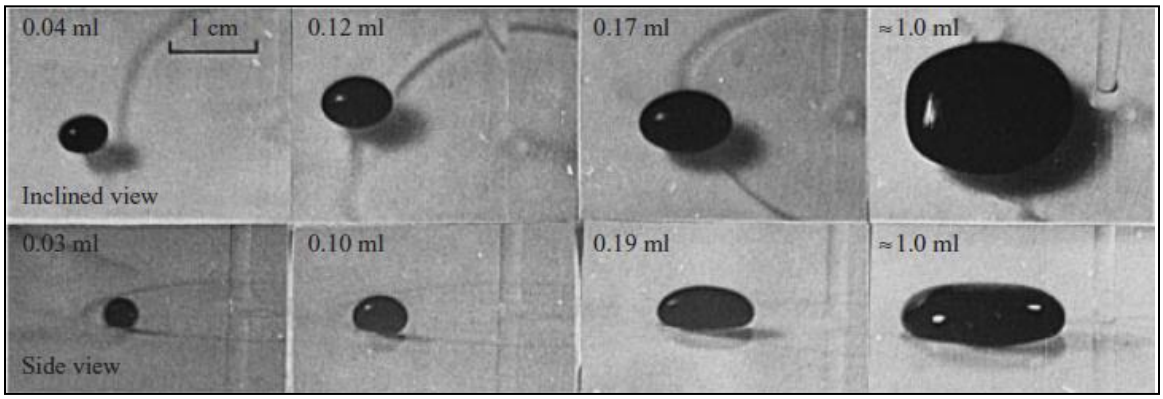

Figure 7: Levitation of a water drop on a hydraulic jump is shown in inclined view (top) and side view (bottom). The numbers in the images are the volume of the drop. The hydraulic jump was created by a vertical water jet hitting a glass plate at about 8 cms^{-1}. Taken from [12]. *Illustrated under "Fair Use" copyright guidelines*.

2.3 Drops bouncing on an oscillating free surface of fluid

Recent experiments by Couder et al. showed that the non-coalescence between a drop and free surface of a fluid bath can be sustained indefinitely if the bath is vibrated vertically [14]. They also found that the floating drop could be increased in size up to several centimeters during bouncing by injecting more fluid into it, upon which the drop could

become stably afloat on the surface of fluid even without the vertical vibrations [14]. In another article, Couder et al. reported that beyond a critical vertical acceleration of the vibrating bath, the drop acquires a rectilinear motion by interacting with the waves on the bath surface caused by the bouncing drop itself [15] (see Figure 8). Protière et al. reported that in the presence of other droplets, interaction takes place among the droplets through their surface waves, which can result in formation of stable orbits or lattice structure of the bouncing drops [16, 17]. This system was further exploited to demonstrate that upon the passage of bouncing droplet through a slit formed by two submerged objects, the distribution of the deviation angles of the droplets is same as that observed in Young's fringes for photons and electrons [18]. Thus, a droplet bouncing on a vertically oscillated bath was shown to demonstrate particularly rich set of features**.**

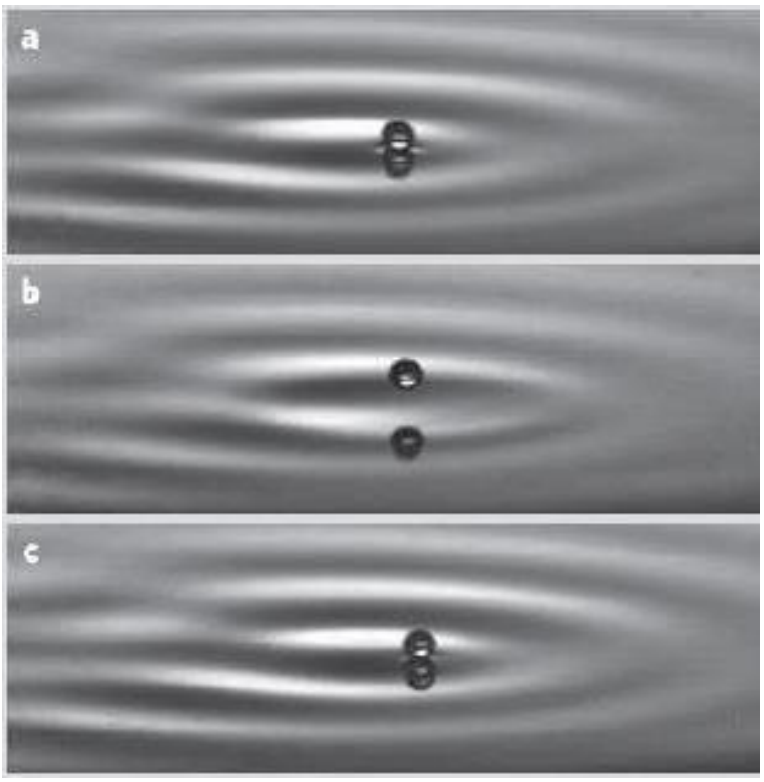

Figure 8: A series of images showing a droplet bouncing over an oscillating fluid bath moves due to interaction with its own wave field generated on the surface. Taken from [15]. *Illustrated under "Fair Use" copyright guidelines.*

2.4 Jet bouncing on free surface of fluid

In another study of non-coalescence between two volumes of same fluid, Thrasher et al. demonstrated the bouncing of a Newtonian fluid jet off a moving bath of same fluid (see Figure 9) [19, 20]. They showed that an air film trapped by the jet separates the jet from the bath fluid and allows it to bounce off without coalescing. This system, as opposed to a drop bouncing off a surface, could be sustained indefinitely, owing to the continuous replenishment of the air film by the moving jet. They proposed simple scaling relationships based on energy arguments which matched well with the experimental data.

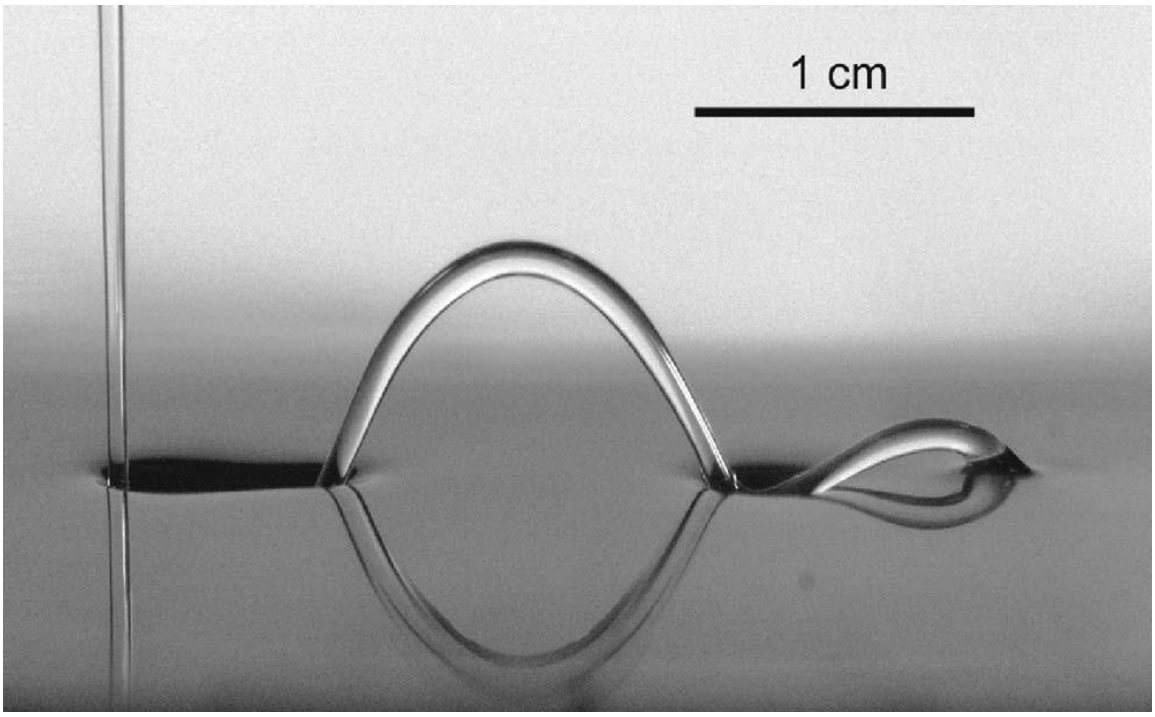

Figure 9: A Newtonian fluid jet bouncing off the surface of a moving bath of same fluid. Taken from [20]. *Illustrated under "Fair Use" copyright guidelines*.

2.5 Drops bouncing on hydrophobic surface

Richard et al. performed high speed filming of drops bouncing on a hydrophobic surface and found that the contact time is independent of the impact velocity, while it increases with the drop radius according to a power law with exponent 1.5 [21]. This showed that the dimensionless contact time of the drop bouncing on a hydrophobic surface scales with the Weber Number (*We*), which is a measure of the relative magnitude of kinetic and surface energies of the drop [21]. In a related study, Clanet et al. carried out a detailed study of the deformation in the drop during the impact using high speed videography measurements and found that for drops in which viscous effects are ignorable, the maximum deformation scales as $We^{0.25}$ [22]. This result, which could not be explained by a simple energy balance, was explained by considering the effective capillary length at

the instant of maximal deformation. Clanet et al. argued that the droplet under maximum deformation behaves as a small puddle of fluid, for which the vertical length scale is approximated by the capillary length [22]. Normally, the capillary length is dependent on the acceleration due to gravity, but in this case, the effective capillary length is determined by the impact acceleration of the drop, which can be several times the acceleration due to gravity. This effective capillary length, combined with volume conservation gave the accurate scaling relationship for the maximal deformation of drop consistent with the experimental observations [22].

2.6 Colliding drops

Bradley and Stow performed a parametric study on collision of droplets with each other and investigated the influence of an impact parameter *X*, which was defined as the ratio of the distance between the trajectories of two droplets and the sum of their radii [23]. Thus $X = 0$ corresponded to a head-on collision while $X = 1$ corresponded to a grazing contact between the drops. They found that the collision frequency decreased with an increase in *X*, as would be expected. They also gave an empirical criterion stating the requirement of coalescence to be $R \leq \frac{1}{4}(3We + 1)$, where *R* is the radius of the droplet and *We* is the Weber number, defined in their study as $We = 2\rho RV^2/\sigma$, where ρ is the density, *V* is the velocity of impact and σ is the surface tension. Moreover they developed a theoretical model for the air film thinning, which matched well with the experimental results and the approximate criterion of $R \leq \frac{1}{4}(3We + 1)$.

Ashgriz and Poo carried out an extensive study on binary collision of liquid droplets with a range of size ratios and impact Weber Numbers [24]. They reported the phase plots

showing boundaries between different regions for coalescence and bouncing. Jiang et al. carried out a similar study for the binary collision between hydrocarbon droplets [25]. Orme wrote a review of the development in colliding droplets work till that time [26]. Qian and Law extended the work of earlier researchers by investigating both water and hydrocarbon droplet collisions and also studied the influence of surrounding gas (molecular properties, density) and the ambient pressure [27]. They found that the collision of both hydrocarbon and water droplets could be divided into 5 distinct categories based on their outcome and they studied the role of Weber number and impact parameter on the outcome of collision [27].

2.7 Colliding bubbles

In a study on the collision of air bubbles in water, Ribeiro and Mewes investigated the role of temperature and electrolyte concentration on the bouncing to coalescence transition parameters, namely the size of bubbles and their relative velocity [28]. Based on their results they proposed an empirical relationship which described how the critical velocity for coalescence varies with the size of bubble. Their results showed that beyond a maximum size of bubbles, the critical velocity for coalescence was independent of the bubbles' size, while below a maximum size, the critical velocity decreased with the bubbles' size [28].

2.8 Drops bouncing on soap film

Courbin & Stone first investigated the bouncing of a drop on a stationary horizontal soap film [29]. They found that for small impact velocities, the droplet bounced on the soap

film while at higher velocities, it passed through the film without breaking it, attributing it to the self-healing properties of soap film, described earlier by Taylor and Howarth [30] and Taylor and Micheal [31]. Gilet and Bush further explored this configuration and studied the impact of drops on stationary and vertically oscillating soap films [32]. For stationary films, they found a several outcomes of the impact, including bouncing, partial coalescence, total coalescence and passing. The outcome of impact was shown to be dependent on the impact Weber Number, though transition from one behavior to the other was not always very crisp. For the cases in which the droplet did bounce on the soap film, they found that the time duration of apparent contact between the droplet and the soap film was independent of the impact speed, while it depended on the mass of the droplet [32].

For impact with oscillating films, they reported several bouncing behaviors, including simple and complex periodic states, and even chaotic behavior. They developed simple theoretical models for the elasticity of soap film and of the energy dissipation in the bouncing droplet, which served well to explain various experimental observations [32].

Chapter 3: Methods and Materials

3.1 Experimental Setup

The experiments were mainly conducted with Silicone oil, which was selected for its stability and well controlled physical properties. As compared to water and other hydrous solutions, silicone oil undergoes much less absorption of impurities from the surrounding air, thus its properties stay much more stable over time. Use of silicone oil also allowed for changing the viscosity of the fluid without changing any other physical properties, which in turn allowed the study of the effect of viscosity alone on the bouncing jets. Silicone oils of viscosity 10, 20 and 50 centistokes (Clearco Products Co., Inc.) were used for the experiments carried out in this study. Silicon oils of all different viscosities have almost the same surface tension, around 20 mN/m. Since silicone oil does not allow us to change the surface tension of the fluid, we performed a few experiments with glycerin/water mixture to study the effect of surface tension on bouncing of jets.

The general setup for the apparatus is shown in Figure 10. Two glass syringes (Poulten and Graf Fortuna™, 50 ml) were filled with Si oil and placed on a syringe pump (NE-4000, New Era Pump Systems, Inc.). Fluid was pushed through the syringes at a prescribed flow rate ranging from 400 ml/hr to 2200 ml/hr, so that it flowed to the stainless steel needles (McMaster-Carr) via PVC tubes. The needles were mounted on two 3-axis translation stages (DT12XYZ - 1/2" XYZ Dovetail Translation Stage, Thorlabs, Inc.), which allowed easy manipulation of the position of needle exit to ensure head on collisions between the jets. The needles were adjusted in such a way that the two jets coming out of the needles were in the same vertical plane and collided soon after

emerging from the needles. After the collision the fluid was collected in a beaker and then reused for the experiments.

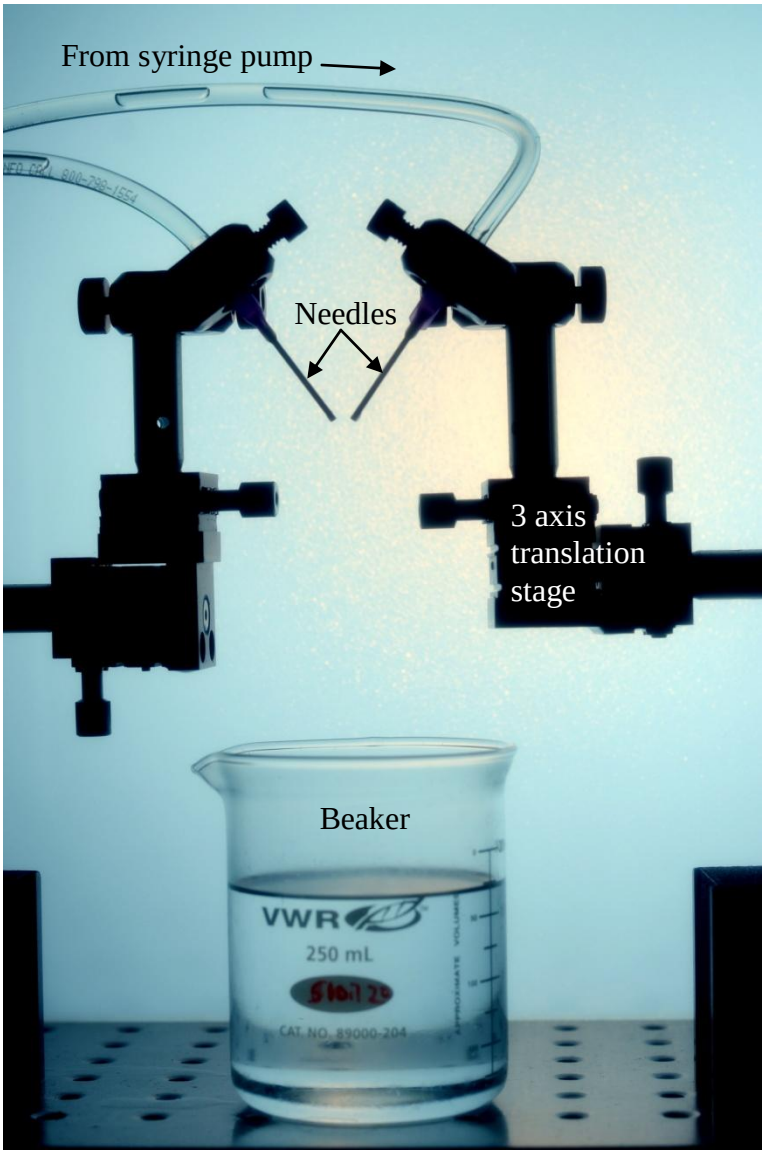

Figure 10: Experimental setup. Two 3 axis translation stages are used for precise positioning of the needles. A syringe pump pushes fluid through two identical needles to form jets. The fluid is collected in a glass beaker after collision.

The diameter of the colliding jets was assumed to be same as the internal diameter of the needles. There was very little change in the size of the jet after exiting from the needle up to the collision. As the jet accelerates due to gravity, its velocity increases and to conserve the volume, diameter decreases. To further avoid any changes in jet size due to increase in velocity, we kept the needle exits close to each other. Needle diameter is dictated by the Gauge number, with the size of needle increasing with a decrease in the corresponding Gauge number. We used stainless steel needles ranging from Gauge 16 (ID 1.35 mm) to Gauge 21 (ID 0.58 mm) for the bouncing jet experiments and Gauge 16 to Gauge 20 (ID 0.65 mm) for the transition experiments. Gauge numbers and internal diameters of all the needles used in this study are listed in Table 1. The velocity of the jets was calculated by dividing the flow rate with the area of the jet.

Table 1: Needle Gauge sizes

Gauge Number	**Internal diameter (mm)**
16	1.35
18	0.97
19	0.81
20	0.65
21	0.58

3.2 Experimental Procedures and Imaging

Two main aspects of the non-coalescence among jets were investigated in this study. In the first set of experiments, the transition of the jets from bouncing to coalescence was investigated. These experiments were conducted using silicone oil with kinematic

viscosity 20 cSt and with needle gauge sizes 16, 18 and 19 (corresponding to ID 1.35, 0.97 and 0.81 mm respectively). A few trial experiments for each jet size and angle indicated the flow rate range in which the transition to coalescence most likely took place. Once the approximate transition region was determined, flow rate was increased from one end of the region to the other end in steps and more careful transition experiments were conducted. In each experiment, after fixing the experimental parameters such as jet size, angle and flow rate, the life-time of bouncing was measured. For each flow rate, several (~ 20) events of bouncing were recorded in order to get accurate statistics. All experiments were video recorded using a Sony camcorder (Model number: HDR-XR100). The videos were later analyzed in VirtualDub video processing/analysis software and the life-time for each bouncing event was measured. The angle α was measured by extracting a frame from the video and analyzing it in the image analysis code described in the next section.

In the second set of experiments, the effect of jet velocity, diameter and angle of inclination on the physical characteristics of the bouncing jets was investigated. For these experiments, a Nikon D7000 digital single-lens reflex camera attached with a Nikon lens (AF NIKKOR 50mm f/1.8D) was used to image bouncing jets. The cameras were aligned perpendicular to the plane containing the two jets. In order to achieve higher magnification, we used a variable number of extension tubes and Nikon PB-4 bellows. The bellows increased the effective focal length of the lens while the distance between the lens and the plane of the jets was reduced. The jets were backlit using a Lowel Pro-Light coming through a diffuser, which provided a uniform backlighting. All images were calibrated using a fine 200 μm× 200 μm calibration mesh (Multi-Grid Standard

Stage Micrometer, Edmund Optics). The camera was triggered using a wired remote trigger cord (Nikon MC-DC2 Remote Release Cord) in order to ensure that the calibration was not disturbed during the experiment.

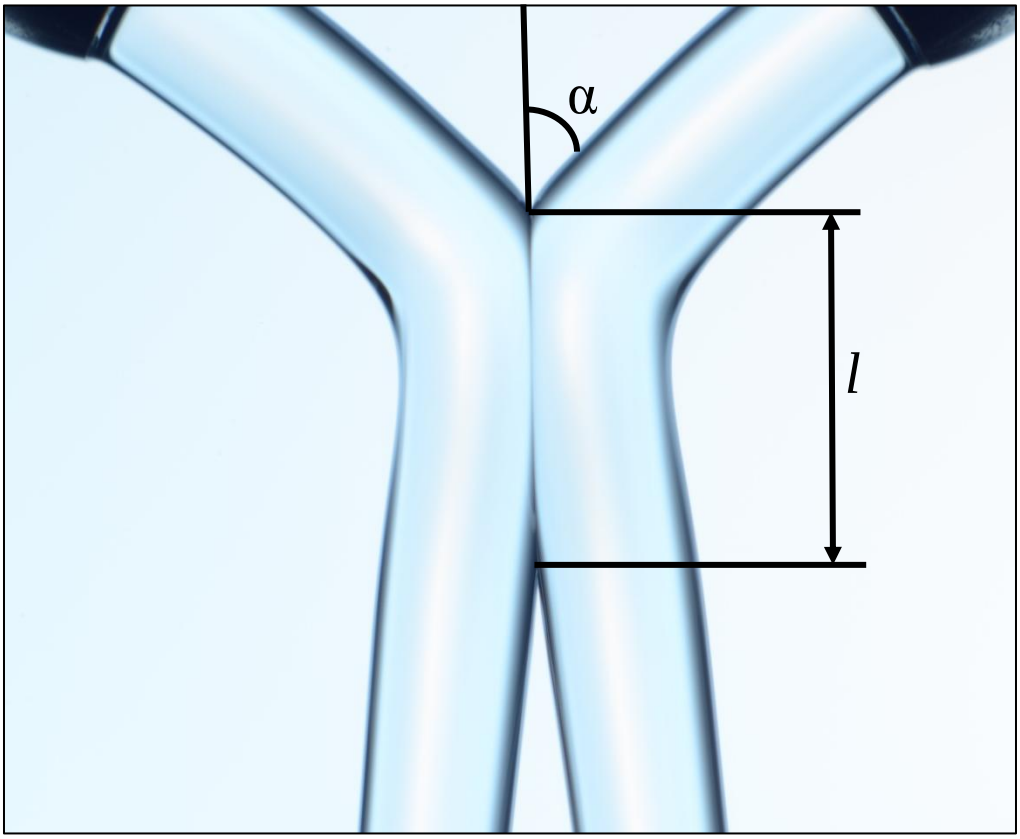

Figure 11: Typical image of bouncing jets showing the quantities of interest; α is the angle between the jet and the vertical axis and *l* is the length of contact region of the bouncing jets

For a fixed combination of needle size and angle, flow rate was increased in steps until the jets started to coalesce in every trial. Multiple images were taken for each set of experimental parameters and the measurements from all these images were used to calculate average values for the physical characteristics of bouncing jets. A typical image from the camera is shown in Figure 11 and is used to illustrate the geometry of the

bouncing jets. The angle that the incoming jets made with the vertical is termed α, while the vertical length of the deformed collision region is called the contact length and termed *l*. These two quantities were measured using digital image analysis, which will be described in greater detail later.

3.3 Image Analysis

The image analysis for this work was carried using custom written MATLAB© code (see Appendix 1). After converting the RGB image into grayscale, the image was converted to binary image. An inbuilt MATLAB© function was then used to trace the upper boundary of the incoming jets and the minimum y-coordinate of the top edge and bottom edge of this boundary was identified (point 1 and point 2 in Figure 12). The mid-point of these two points was used as the point of collision between the two jets. Then a similar method was employed on the lower boundary of the jet to identify the point of separation of the jets (midpoint between point 3 and point 4 in Figure 12). The contact length of the jets was thus measured as the distance between these two points. The angle α was measured from the above mentioned points in combination with appropriate points on the boundary of the jets (blue circles in Figure 12). The point on top right allows the measurement of incoming angle of the jet on the right, and point on top left allows the measurement of incoming angle of the left jet. While both angles were measured, the incoming angle of the jet on the right was used as the angle α. Similarly, the angles between the jets and the vertical were measured after the collision, even though these haven't been used in the present study.

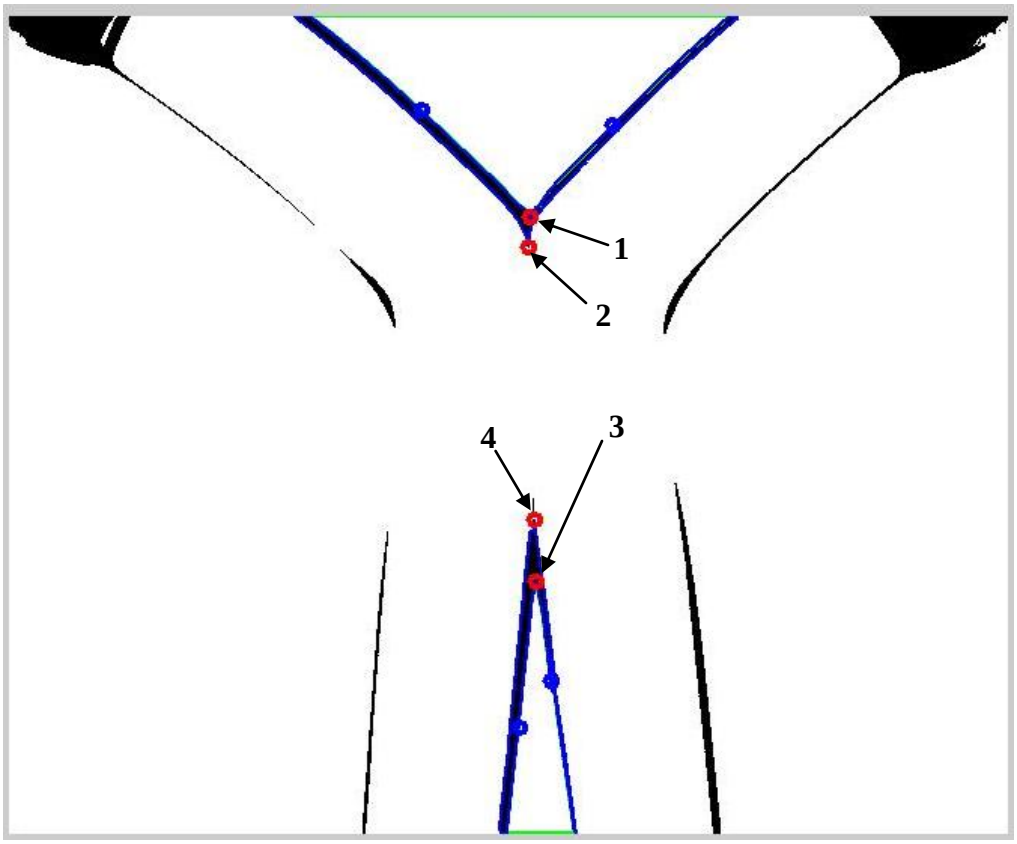

Figure 12: Snapshot of the image analysis code output. Midpoint between points 1 and 2 gives the point where the collision starts, while midpoint between points 3 and 4 is the point where the jets separate.

Chapter 4: Results and discussion

4.1 Transition from non-coalescence to coalescence

In the first part of the study, criteria that govern whether or not the jets bounce upon collision were examined. For this purpose, a study of transition of the colliding jets from bouncing to coalescence was investigated. In these experiments, after fixing a needle size and angle, flow rate was increased in steps and the life-time of bouncing of the jets was noted. For a given set of experimental parameters, the pump was started and the flow was allowed to develop to the set velocity. Once the jets coalesced, they were perturbed using a needle and bouncing was thus re-initiated (see Figure 13). The experiments were video-recorded and the life-time of such bouncing was measured from the videos as the time taken from initiation of bouncing by perturbation to eventual coalescence of jets. Observations were repeated several times to calculate the center and spread in the distribution of bouncing life-time. In most cases, around 20 observations were used for statistical measures and in no case, less than 10 observations were used. Sample size was sometimes smaller than 20 for the small jet velocities in which the bouncing lifetime was so high that the syringes would run out of fluid before enough observations were made.

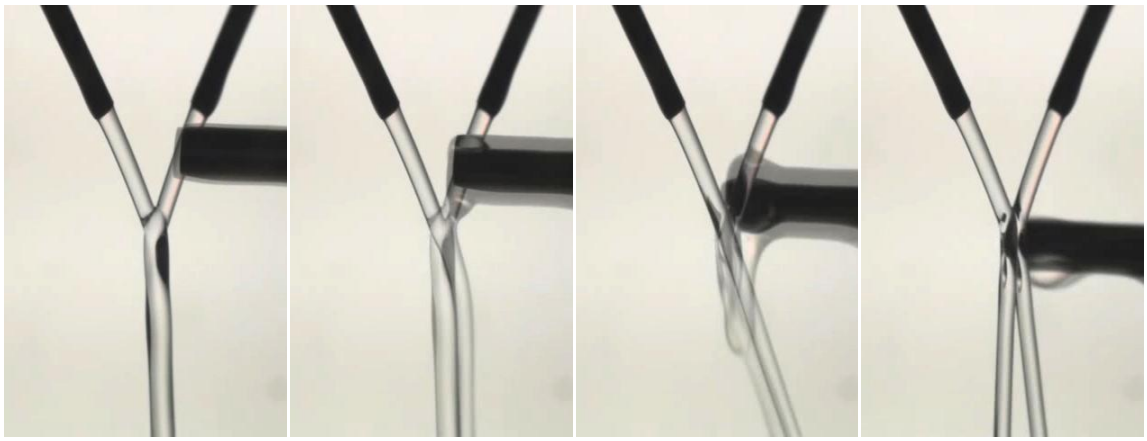

Figure 13: Series of images show the re-initiation of bouncing by perturbation of two coalesced jets using a needle.

The distribution of bouncing life-time was usually not normal, especially for the small jet velocities. There were often a few outlier observations which strongly affected the mean and the standard deviation of the bouncing life-time distribution. For this reason, median and the Median Absolute Deviation (MAD) were used as representatives of center and spread of the distribution respectively.

If the flow rate for certain jet diameter and angle was such that the velocity was jet was not beyond the critical velocity for bouncing, the coalescence was caused by random chance events such as disturbances, dirt etc. In this situation, the median life-time of bouncing was high and the MAD of the bouncing life-time was also high. As the flow rate and thus the jet velocity was increased, the median as well as MAD of the bouncing life-time rapidly decreased. After a critical jet velocity, no bouncing events were observed upon several repeated perturbations. The life-time of bouncing for these jet velocities was thus declared equal to zero if no bouncing was observed after 20 perturbations.

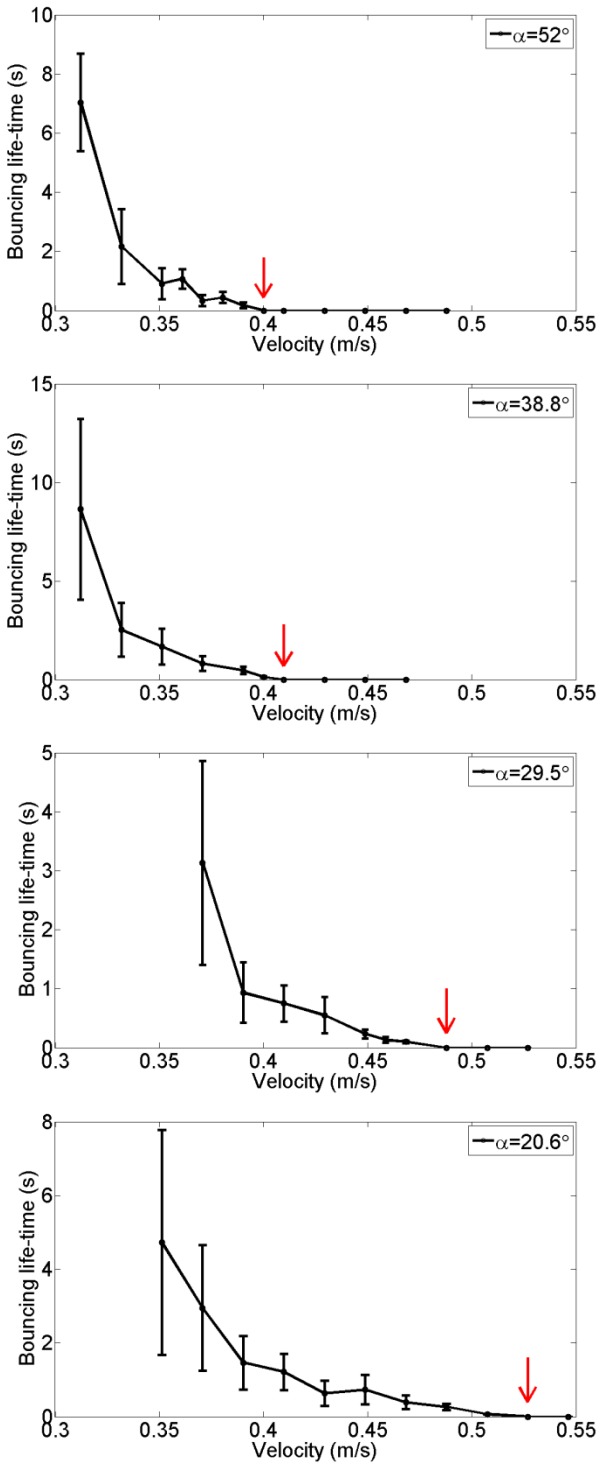

Figure 14: Bouncing life-time versus jet velocity for different jet angles in Gauge 16 experiments. Points denote the median life-time of bouncing while the error bars are of length equal to half of MAD on each side. Red arrows indicate transition velocity.

Figure 14 shows the plots for the bouncing life-time measured with needles of gauge size 16 against jet velocity for different jet angles α. The length of error bars represents one MAD. It can be easily noted in Figure 14 that for smaller jet velocities, the median life-time of bouncing is significantly higher than that for higher velocities, and it shows the same downward trend for all different angles. Also, the MAD in the bouncing life-time decreases as the velocity of the jet increases. In all cases of jet angle α, a critical jet velocity can be identified beyond which there is no bouncing and thus the life-time of bouncing is zero. This velocity is taken to be the transition velocity from bouncing to coalescence for the given jet angle.

Figure 15 shows the plot of transition velocity versus the jet angle α for gauge 16 needles. It shows that as the jet angle increases, the transition velocity decreases. In terms of the hypothesis mentioned earlier this behavior can be easily rationalized. For a fixed flow rate, the normal component of the jet increases with an increase in jet angle α with respect to the vertical. An increase in normal velocity will result in an increase in the contact time $T_{contact}$ of the bouncing jets while it should result in a decrease in the drainage time $T_{drainage}$ of the air film between the two jets. Thus, there will be a transition from bouncing to coalescence with an increase in angle α for a fixed jet velocity. If looked from the perspective of velocity, for a fixed jet angle α, the transition will take place at a smaller jet velocity if the jet angle α is large. That is exactly the trend that is seen in Figure 15. A quantitative explanation of the trend observed will require an accurate modeling of the drainage time $T_{drainage}$ to understand how that changes with a change in the jet velocity and jet angle.

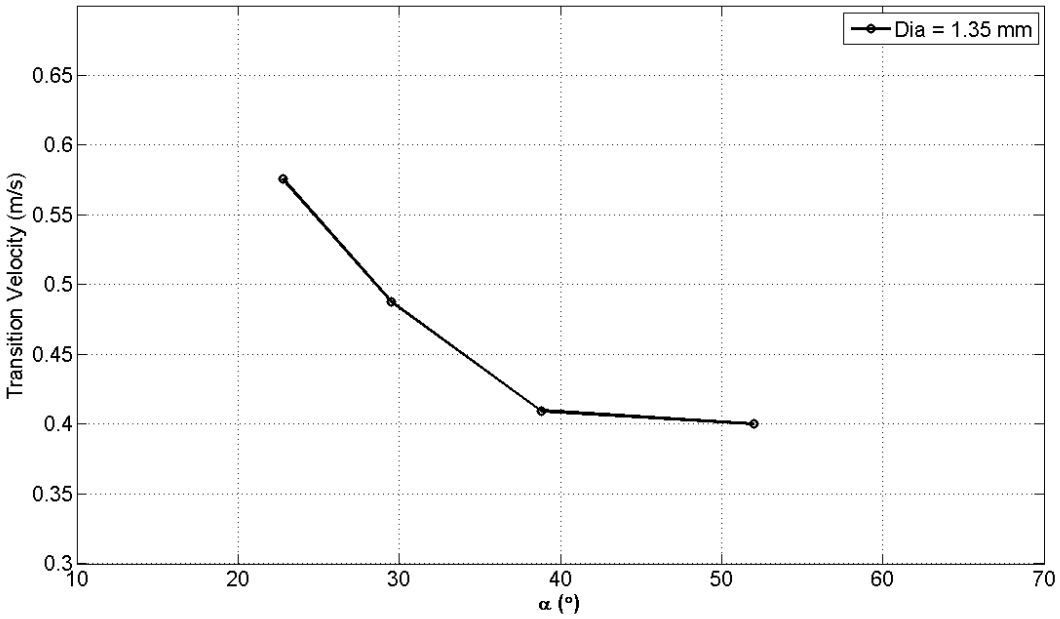

Figure 15: Transition velocity versus jet angle α for Gauge 16. The critical velocity required for coalescence decreases as α increases.

In the same manner as for gauge 16, transition experiments were carried out with Gauge 18 and Gauge 19 to study the effect of jet diameter on the transition from bouncing to coalescence. In these cases, a critical jet velocity for transition was determined without a detailed analysis of bouncing life-time as the minimum velocity for a given jet angle above which no bouncing events were observed in 20 perturbations. Having determined the transition velocity for different jet angles with Gauge 18 and 19, transition curves could be plotted for these two jet sizes.

For Gauge 18, transition experiments were carried out with 5 different jet angles ranging from 21° to 51° and the critical velocity was determined above which no bouncing was observed. Figure 16 shows the plot of transition velocity versus jet angle for Gauge 18. It can be seen that the transition curve for Gauge 18 shows a similar trend as Gauge 16; the

transition velocity decreases as the jet angle increases, resulting from an increase in the contact time $T_{contact}$ and reduction in the drainage time $T_{drainage}$.

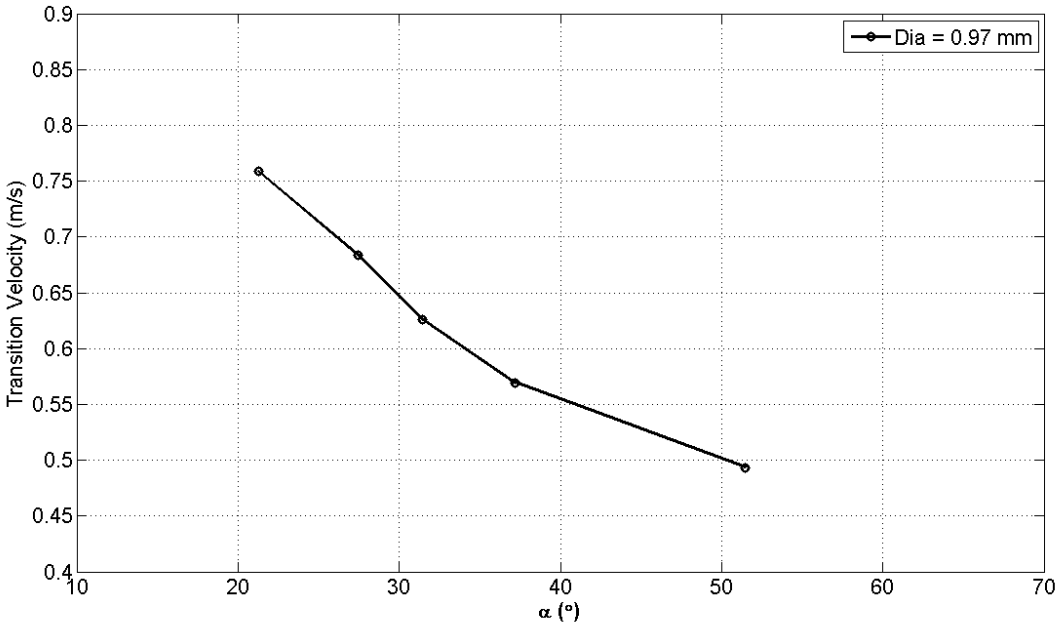

Figure 16: Transition velocity versus jet angle α for Gauge 18. The critical velocity required for coalescence decreases as α increases.

In the case of Gauge 19, the syringe pump started getting stalled at higher flow rates as a large force was required to push the fluid through the small sized needle. For this reason, transition velocities could only be determined for the larger jet angles (α > 30°) as the transition velocity for smaller angles was higher than the maximum velocity at which the pump could function. Four different jet angles were examined for the transition from bouncing to coalescence. The transition curve for Gauge 19, with four data points for four angles, is shown in Figure 17. Trend seen in Figure 17 is same as that seen for the other

two needle sizes; the transition velocity decreases with an increase in the jet angle as expected from the contact time versus drainage time hypothesis.

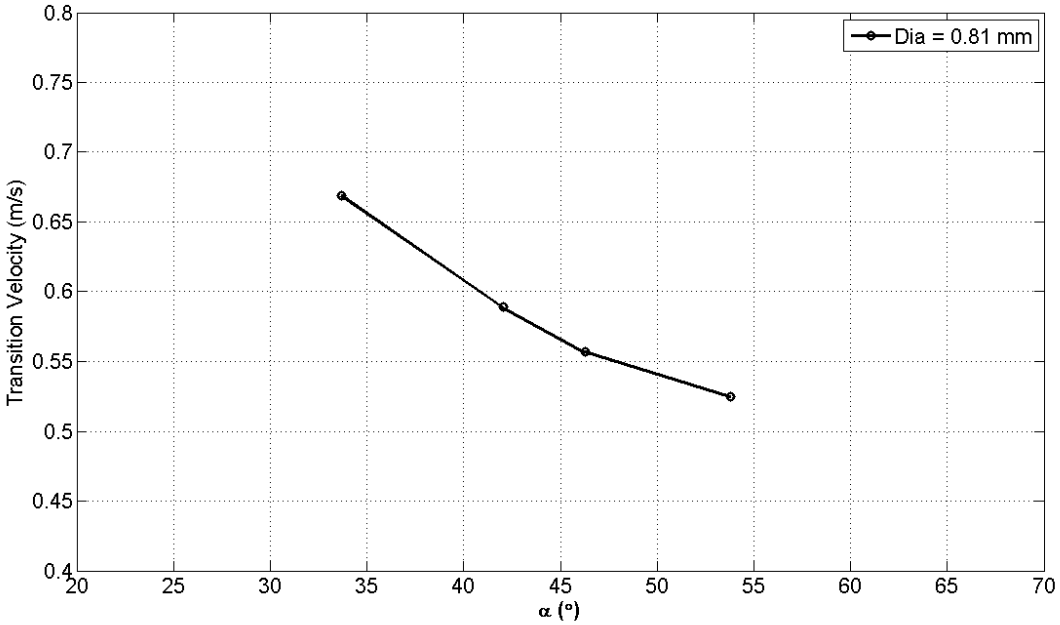

Figure 17: Transition velocity versus jet angle α for Gauge 19. As seen in the transition curves for other needle sizes, the transition velocity decreases as α increases.

When the transition curves for different needle sizes are plotted together, as shown in Figure 18, they reveal that the transition curves for different jet sizes are almost parallel to each other and show a systematic trend. It is noted that the transition velocities increase for the same jet angle as the jet size decreases (higher gauge numbers correspond to smaller jet size).

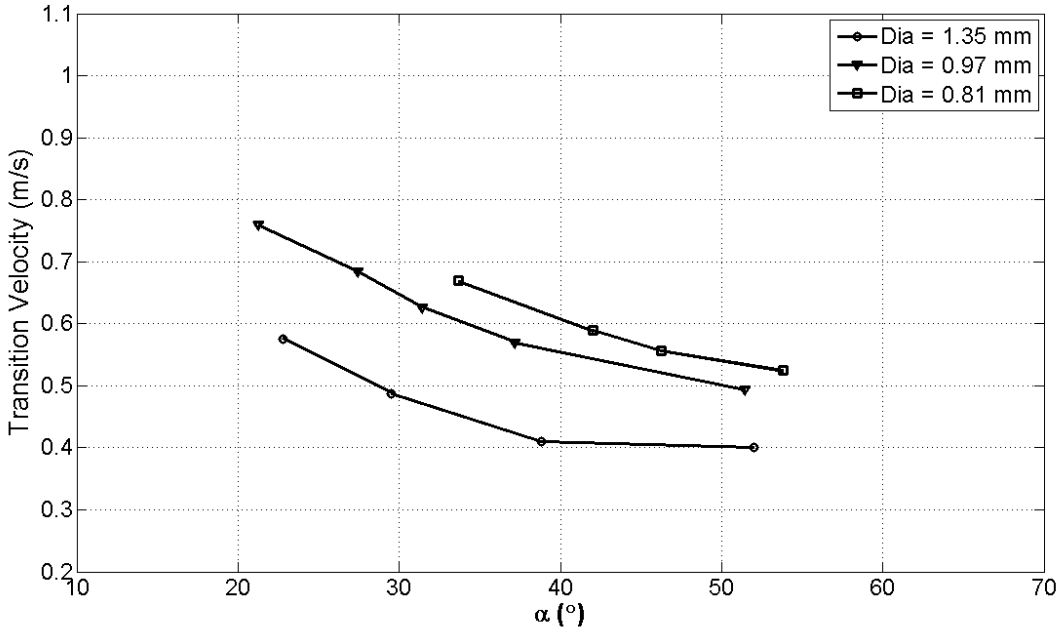

Figure 18: Transition velocity versus jet angle α for Gauges 16, 18 and 19. The transition curves for different needle sizes shows similar trends and lie almost parallel to each other.

In order to rationalize the results obtained from the transition experiments, a form of the Normal Weber Number is used, represented by $We_{\perp}$, different from that defined later in Section 4.2. A characteristic length scale, the dimension of the jet in a plane parallel to the plane of collision, is used to define $We_{\perp}$. This length scale is equal to $\frac{D}{\sin\alpha}$, as shown in Figure 19 below.

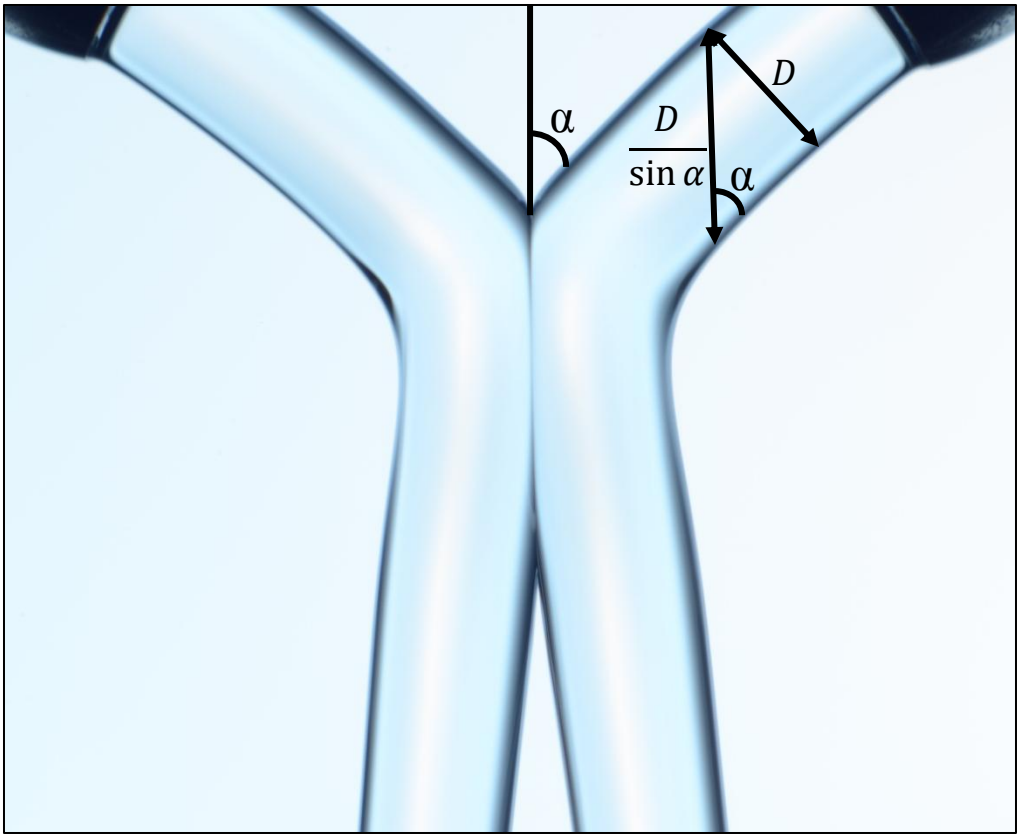

Figure 19: Characteristic length scale used to define the Normal Weber Number $We_{\perp}$.

Using $\frac{D}{\sin\alpha}$ as the characteristic length scale and the normal velocity $V\sin\alpha$ as the characteristic velocity scale in the definition of Normal Weber Number $We_{\perp}$, we get

$$We_{\perp} = \frac{\rho(V\sin\alpha)^2}{\sigma} \times \frac{D}{\sin\alpha} = \frac{\rho V^2 D\sin\alpha}{\sigma} \qquad (1)$$

Using this definition of Normal Weber Number $We_{\perp}$, the observations from all different experiments were plotted with $We_{\perp}$ on the Y- axis and jet angle α on the X- axis, as shown in Figure 20. The observations in which no bouncing was observed were plotted with red symbols and the ones in which bouncing was observed were plotted with black

symbols. Different shapes were used for different needle sizes – circles for Gauge 16, triangles for Gauge 18 and diamonds for Gauge 19.

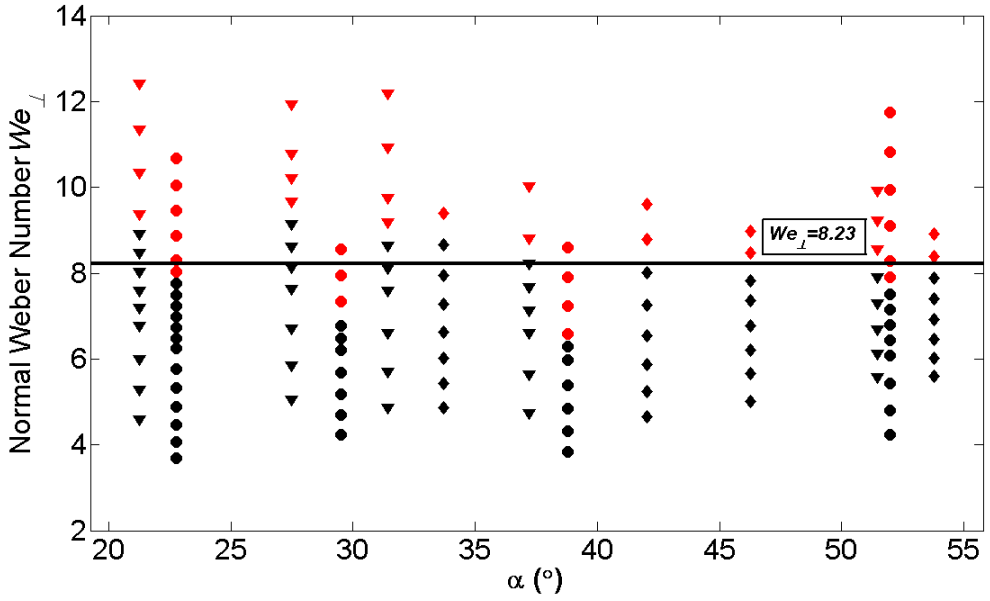

Figure 20: Normal Weber Number $We_\perp$ versus jet angle α for Gauge 16 (circles), 18 (triangles) and 19 (diamonds). Black markers represent bouncing and red markers represent coalescence cases. Horizontal line represents the critical Normal Weber Number $We_\perp^*$ = 8.23, at which the transition from bouncing to coalescence takes place.

Figure 20 clearly shows a critical Normal Weber Number $We_\perp^*$ = 8.23, above which the colliding jets undergo coalescence and below which they bounce from each other. $We_\perp^*$ = 8.23 is calculated as the average of the Normal Weber Numbers at which the transition takes place for all different observations. Even though Figure 20 contains data for different jet sizes and many different jet angles, the transition from bouncing to coalesce for all of them takes place around a critical $We_\perp^*$ = 8.23. That $We_\perp^*$ = 8.23 gives an accurate criteria for the transition from bouncing to coalescence is also evident if the transition velocities for different angles and needle sizes are back calculated from the

$We_{\perp}^{*}$ and plotted next to the experimentally observed transition velocities. Transition velocity for a given jet size and angle is given by

$$V^{*} = \sqrt{\frac{We_{\perp}^{*}\sigma}{D \sin \alpha}} \tag{2}$$

Figure 21 shows the plot of transition velocity against jet angle α for different needle sizes, with the experimentally observed transition velocity plotted with solid line and the transition velocity calculated from Equation 2 plotted with a dashed line. As can be seen in Figure 21, there is a fairly good agreement between the experimental and calculated transition velocities, both in the values as well as in the trends observed.

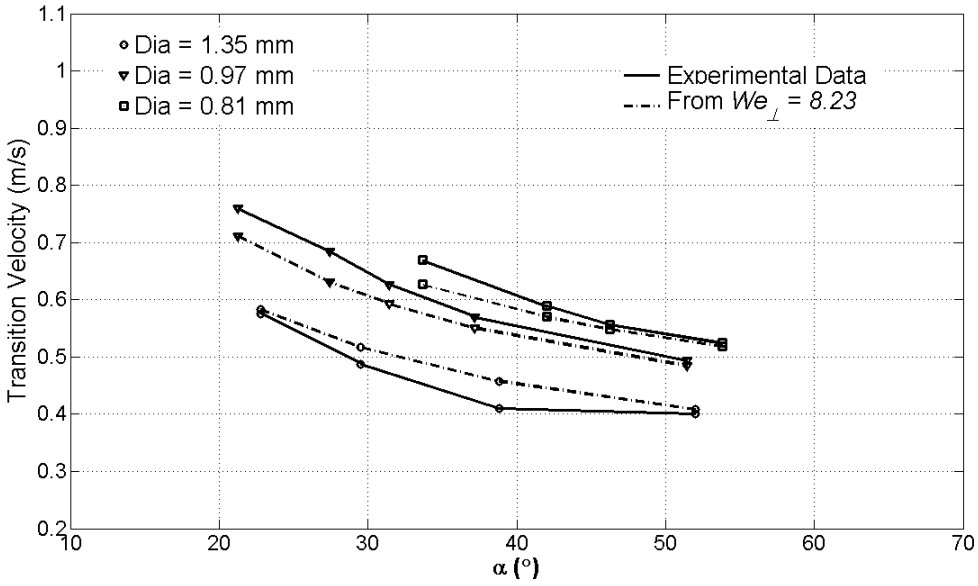

Figure 21: Transition velocity versus jet angle α for Gauges 16, 18 and 19. Solid lines represent experimentally determined transition velocities and dashed lines represent those calculated from critical Normal Weber Number $We_{\perp}^{*}$ = 8.23.

4.2 Contact time of bouncing jets

From the experimental images, an example of which is shown in Figure 11, the contact time scale can be measured by dividing the contact length l with the vertical component of the jet velocity $V\cos\alpha$, where α is the angle between the jet and the vertical. This and can be written as

$$T_{contact} = \frac{l}{V\cos\alpha} \tag{3}$$

The contact time of the bouncing jets can thus be measured for all experiments and can further be converted into its dimension-less form $T^*_{contact}$ by multiplying with the velocity of the jets V and dividing by the diameter of the jets D, i.e.

$$T^*_{contact} = \frac{T_{contact} \times V}{D} \tag{4}$$

The contact time $T_{contact}$ can be derived from scaling arguments, from a balance between inertia and surface tension or from a balance between inertia and viscous forces. If the normal component of inertia (of the order of $\rho(V\sin\alpha)^2 D^3$, with $V \sim \frac{D}{T_{contact}}$) is balanced with surface tension (of the order of σD^2), then we get $T_{contact} \approx \left(\rho D^3 (\sin\alpha)^2 / \sigma\right)^{1/2}$.

In a dimensionless form, the above scaling for $T_{contact}$ can be written as $T^*_{contact} \approx We^{1/2}$, where We is the Normal Weber Number. Normal Weber number (We) is the ratio of normal inertial forces in the jet to the surface tension forces and is defined as

$$We = \frac{\rho(V \sin \alpha)^2 D}{\sigma} \tag{5}$$

where ρ is the density of the fluid, V is the velocity and D is the diameter of the jet. We >> 1 signifies the dominance of inertial effects over surface tension forces, while We << 1 signifies that inertia is negligible as compared to surface tension effects.

On the other hand, if inertia is balanced by viscous dissipation (of the order of $\mu D^3 \sin \alpha / T_{contact}$), then we get $T_{contact} \approx \rho D^2 \sin \alpha / \mu$ or $T^*_{contact} \approx Re$, where Re is the Normal Reynolds Number, defined as

$$Re = \frac{\rho(V \sin \alpha) D}{\mu} \tag{6}$$

where ρ, V and D are the same as defined above, and μ is the dynamic viscosity of the fluid. Large value of Re means that inertial forces dominate viscous effects while a small value of Re (typically Re << 1) indicates that viscous forces are dominant and the flow in this regime is termed as stokes flow.

From the bouncing jets experiments, the contact length of the collision region was measured for various combinations of experimental parameters, and the contact time was then calculated using Equation 3 and non-dimensionalized using Equation 4. Figure 22 shows the plot of dimensionless contact time against the normal Weber number of the colliding jets for ν = 10 cSt. For this and the subsequent plots of dimensionless contact time, the size of the dot on the plot represents the size of the needle used in the experiment, with larger dots representing larger jet diameters. It should, however, be noted that there is no quantitative relationship between the dot sizes and jet sizes, only the order of sizes corresponds to the order of jet sizes. Also, in the plots for dimensionless

contact time, black dots have been used for data from 10 cSt experiments and blue dots have been used for the data from 50 cSt experiments.

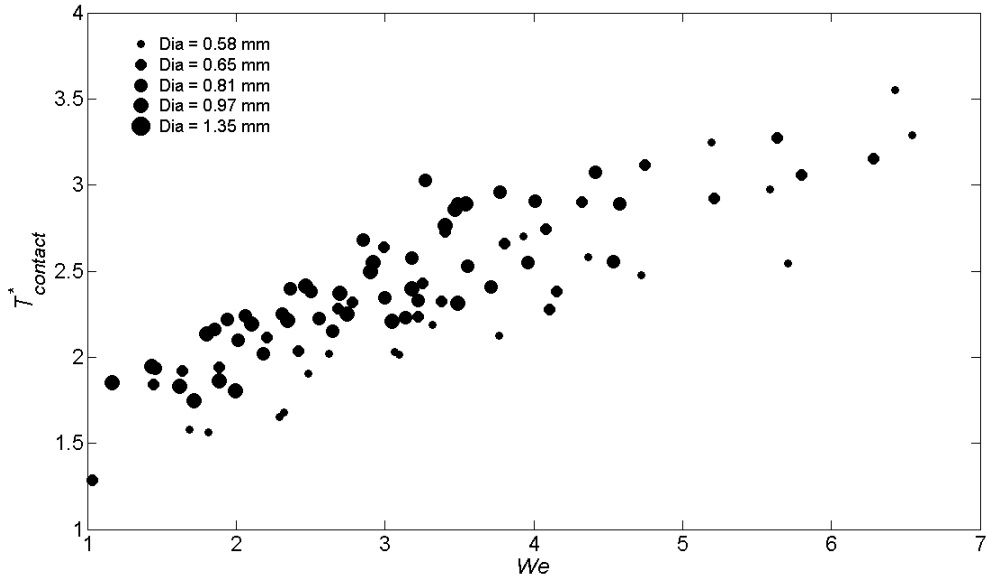

Figure 22: Scatter plot of dimensionless contact time ($T^*_{contact}$) against Normal Weber Number (We) for ν = 10 cSt. Size of dots correlates with the size of jets, but there is no quantitative relationship between the sizes.

As can be seen in Figure 22, data points for all different jet sizes collapse on top of each other and form a narrow band. The dimensionless contact time increases monotonously with an increase in the Normal Weber Number. The plot of dimensionless contact time against Normal Weber Number for ν = 50 cSt, in Figure 23, shows the same trends as observed in the plot for ν = 10 cSt. It can be seen that the data again collapses in one narrow band and the dimensionless contact time increases monotonously with the Normal Weber Number.

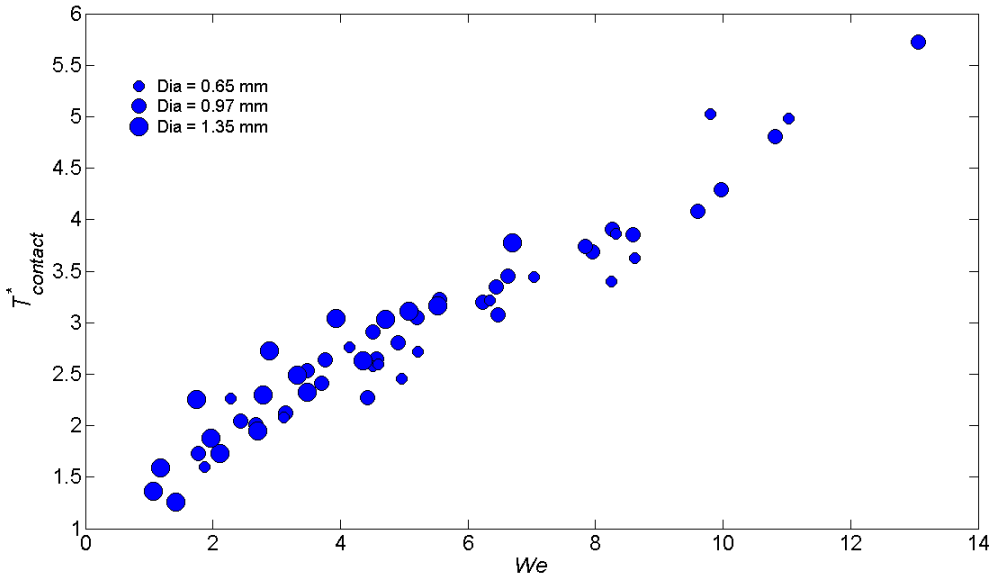

Figure 23: Scatter plot of dimensionless contact time ($T^*_{contact}$) against Normal Weber Number (We) for ν = 50 cSt.

Plots of dimensionless contact time against the Normal Reynolds Number for ν = 10 cSt and 50 cSt are shown in Figure 24 and Figure 25 respectively. It can be noted that these plots show the same trends as the plots of $T^*_{contact}$ against Normal Weber Number. But at the same time, there is much more spread in these plots as compared to those with Normal Weber Number on the x-axis.

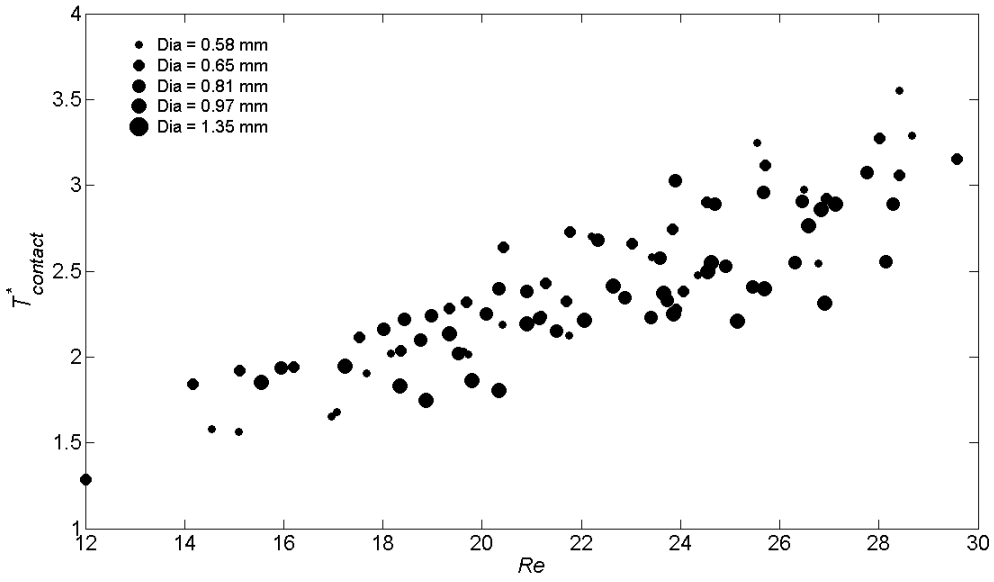

Figure 24: Scatter plot of dimensionless contact time ($T^*_{contact}$) against Normal Reynolds Number (Re) for ν = 10 cSt.

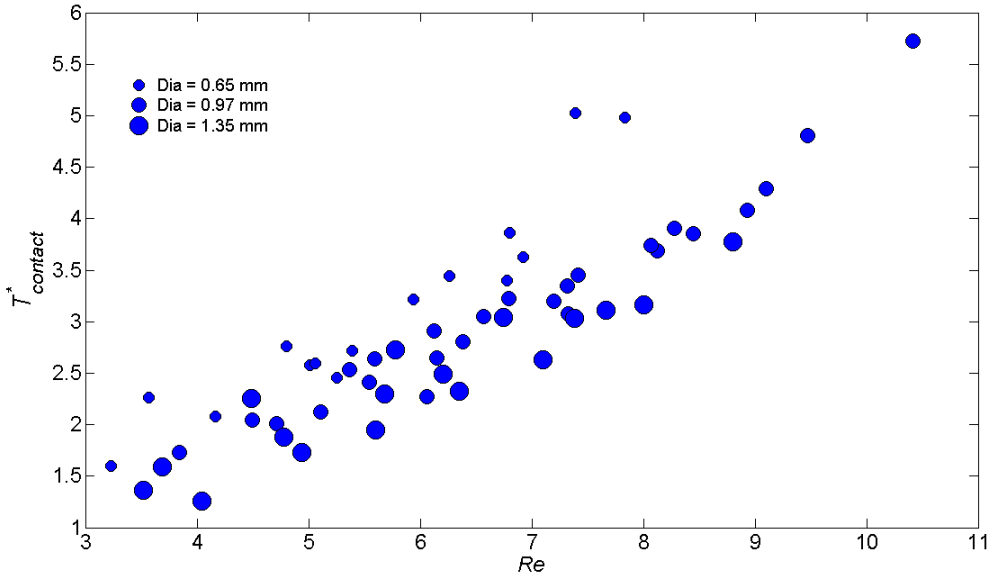

Figure 25: Scatter plot of dimensionless contact time ($T^*_{contact}$) against Normal Reynolds Number (Re) for ν = 50 cSt.

Similarity of the trends in the Normal Weber Number and Normal Reynolds Number plots is not completely unexpected. Since all other parameters in these plots stay the

same, it demonstrates the normal velocity and diameter dependence of the dimensionless contact time and thus both show similar trends. In order to distinguish between the normal Reynolds number and the normal Weber number as the true scaling parameter, some other experimental parameter needs to be changed within the same plot which can differentiate between Normal Reynolds Number and Normal Weber Number dependence. Thus, data for ν = 10 cSt and ν = 50 cSt is plotted together, to see for which of the two dimensionless numbers the trends in data are sustained.

Figure 26 shows the plot of dimensionless contact time verses Normal Reynolds Number for both ν = 10 cSt and ν = 50 cSt. It can be seen that the data for the two different viscosities form two separate bands and do not collapse on top of each other. Moreover, the trends of data in the two bands are very different from each other. This suggests that dimensionless contact time of bouncing jets does not scale with the Normal Reynolds Number and thus the role of viscosity in determining the dimensionless contact time can be rejected.

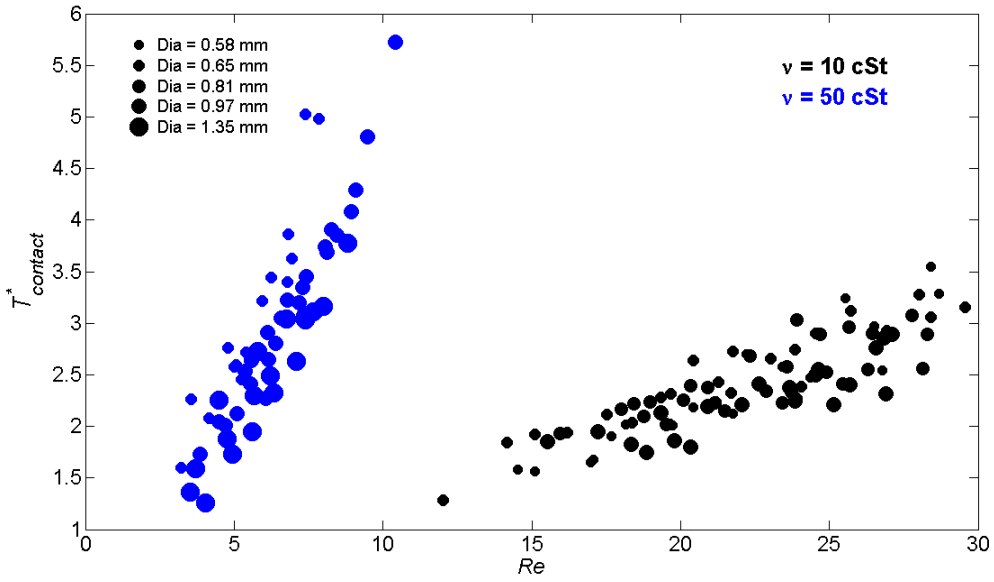

Figure 26: Scatter plot of dimensionless contact time ($T^*_{contact}$) against Normal Reynolds Number (Re) for ν = 10 cSt (black dots) and ν = 50 cSt (blue dots).

On the other hand, if we plot together the dimensionless contact time verses Normal Weber Number for ν = 10 cSt and ν = 50 cSt, all the data collapse together, as shown in Figure 27. The trends of dimensionless contact time for both ν = 10 cSt and ν = 50 cSt are the same and data from both sets have same values of dimensionless contact time for same value of the Normal Weber Number. This shows that the dimensionless contact time of bouncing jets scales with the Normal Weber Number.

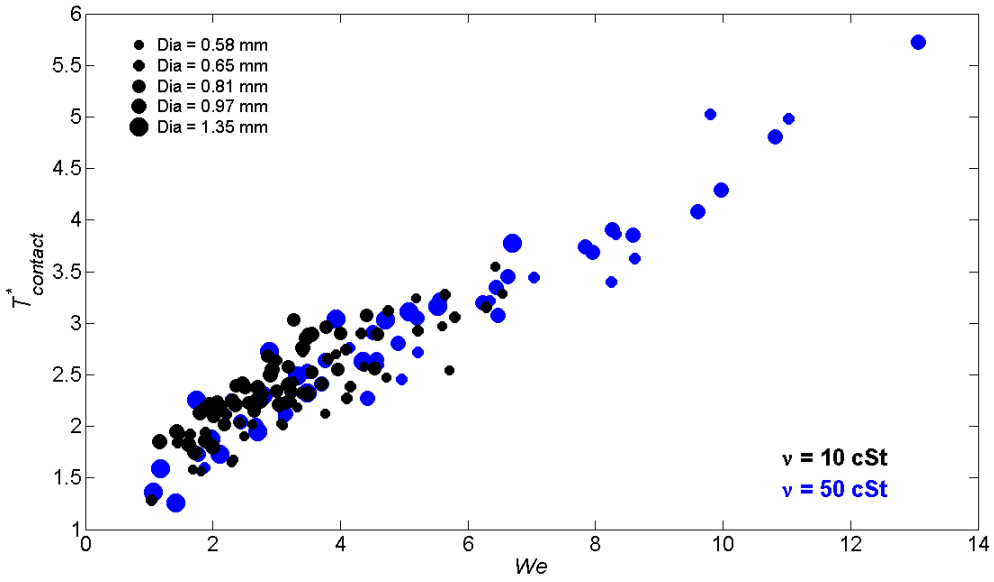

Figure 27: Scatter plot of dimensionless contact time ($T^*_{contact}$) against Normal Weber Number (We) for ν = 10 cSt (black) and ν = 50 cSt (blue).

In order to determine the scaling exponent of the relationship between dimensionless contact time and Normal Weber number, they are plotted against each other on logarithmic axes and slope of a straight line fit on the data is determined, which gives the exponent of the power law relationship between the dimensionless contact time and Normal Weber Number. This plot is shown in Figure 28, which shows a straight line fits well on all the data. Slope of the straight line is found to be 0.467.

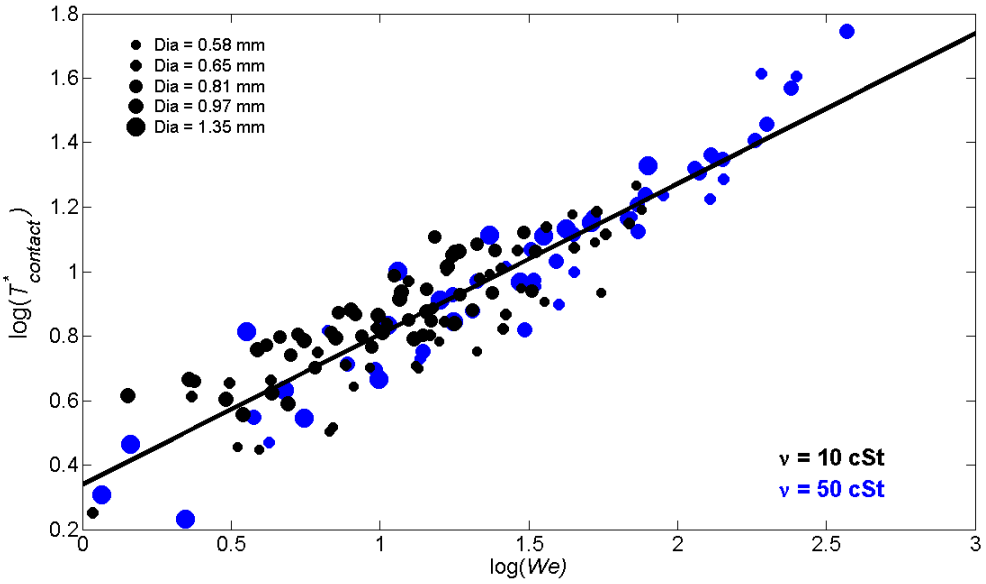

Figure 28: Logarithmic plot between dimensionless contact time ($T^*_{contact}$) against Normal Weber Number (We) for ν = 10 cSt (black) and ν = 50 cSt (blue). Straight line is the best fit line on the data with slope = 0.467, confidence bounds = (0.4336, 0.4997), R^2 = 0.85.

To further check the scaling of dimensionless contact time with Normal Weber Number, experiments were conducted with 75% by weight Glycerol solution which has very different value of surface tension than the silicone oils that were used for the previous experiments but it has similar value of viscosity. The surface tension and kinematic viscosity of 75% by weight Glycerol solution were determined from published data to be 66.1 mN/m and 22.44 cSt respectively [33, 34].

The bouncing of Glycerol solution jets was very unstable due to which it was very hard to conduct experiments with it, and only two data points could be obtained for the 75% by weight Glycerol solution. Figure 29 shows the dimensionless contact time plotted against the Normal Weber Number including the measurements from the Glycerol experiments. It shows that the data points from Glycerol experiments lie very close to the data from

silicone oil experiments and the exponent for the power law scaling including the Glycerol data is found to be equal to 0.462.

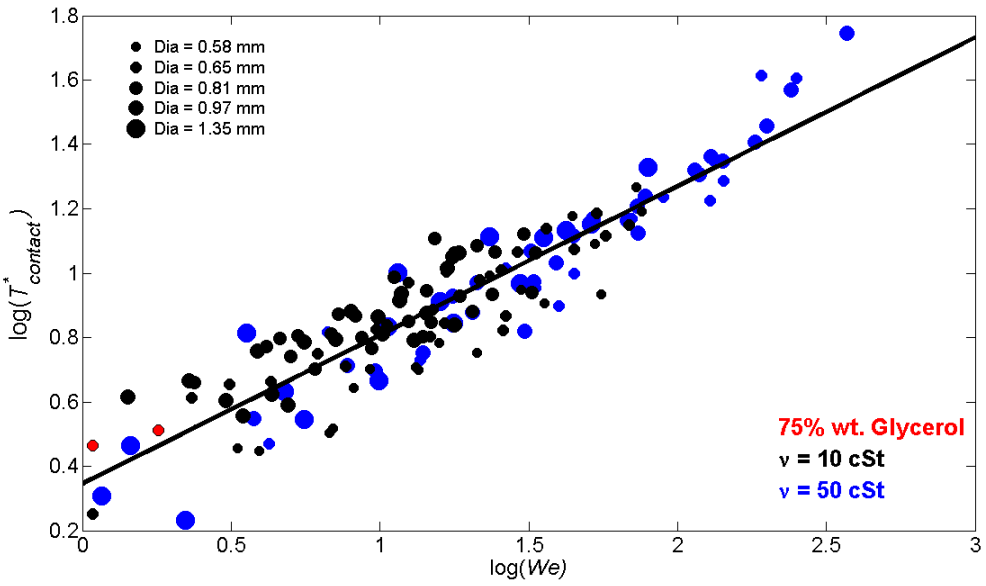

Figure 29: Logarithmic plot between dimensionless contact time ($T^*_{contact}$) against Normal Weber Number (We) for ν = 10 cSt (black), ν = 50 cSt (blue) and 75% by weight glycerol solution. Straight line is the best fit line on the data with slope = 0.462, confidence bounds = (0.4302, 0.4942), R^2 = 0.85.

From Figure 29, it is found that the exponent of the Normal Weber Number scaling from experimental data is 0.4622, which is very close to an exponent of 0.5 as expected from the scaling argument based on balance between inertial forces and surface tension forces. It can thus be deduced from the experimental results that the dimensionless contact time scales as the square root of the Normal Weber Number, i.e.

$$T^*_{contact} \sim We^{1/2} \sim \left(\frac{\rho(V\sin\alpha)^2 D}{\sigma}\right)^{1/2} \tag{7}$$

By writing out the expression for $T^*_{contact}$ from Equation 4 and rearranging the terms, we can get

$$\frac{T_{contact}}{\sin\alpha} \sim \left(\frac{\rho}{\sigma}\right)^{1/2} D^{3/2} \tag{8}$$

Equation 8 suggests that the quantity $\frac{T_{contact}}{\sin\alpha}$ is independent of the jet velocity and scales with the jet diameter with an exponent of 1.5. Figure 30 shows the plot of $\frac{T_{contact}}{\sin\alpha}$ verses the jet velocity V. It can be seen that for a fixed jet size, $\frac{T_{contact}}{\sin\alpha}$ stays almost constant with changing jet velocity, thus confirming that it is independent of the jet velocity.

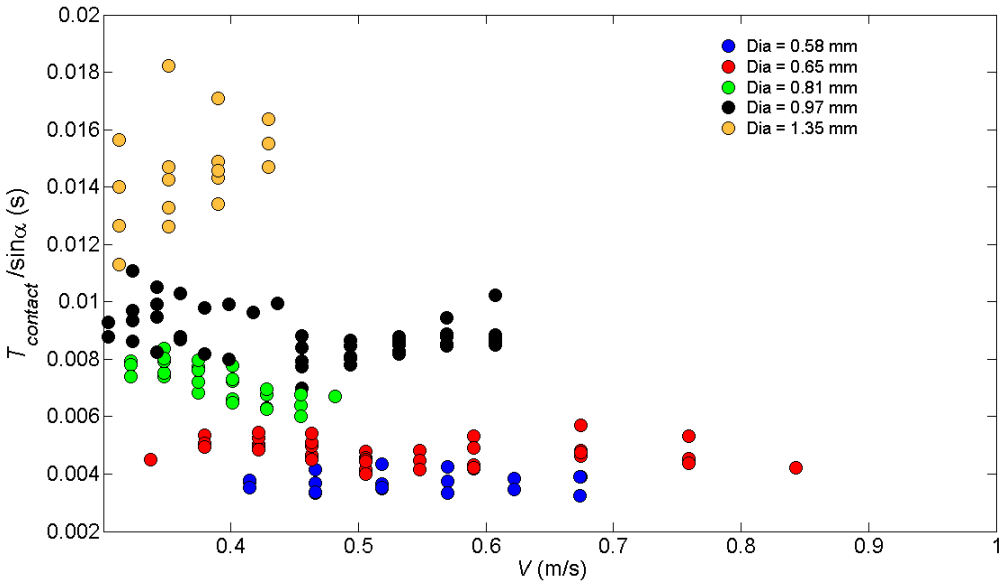

Figure 30: $\frac{T_{contact}}{\sin\alpha}$ verses the jet velocity *V*. Data points for different jet sizes are denoted by different colors and show no trend with change in the jet velocity.

The plot of $\frac{T_{contact}}{\sin\alpha}$ against jet diameter with logarithmic axes is shown in Figure 13. When fitted by a straight line, the data shows a slope of 1.53 on the logarithmic scale, which confirms that $\frac{T_{contact}}{\sin\alpha}$ indeed scales as the jet diameter raised to a power of 1.5.

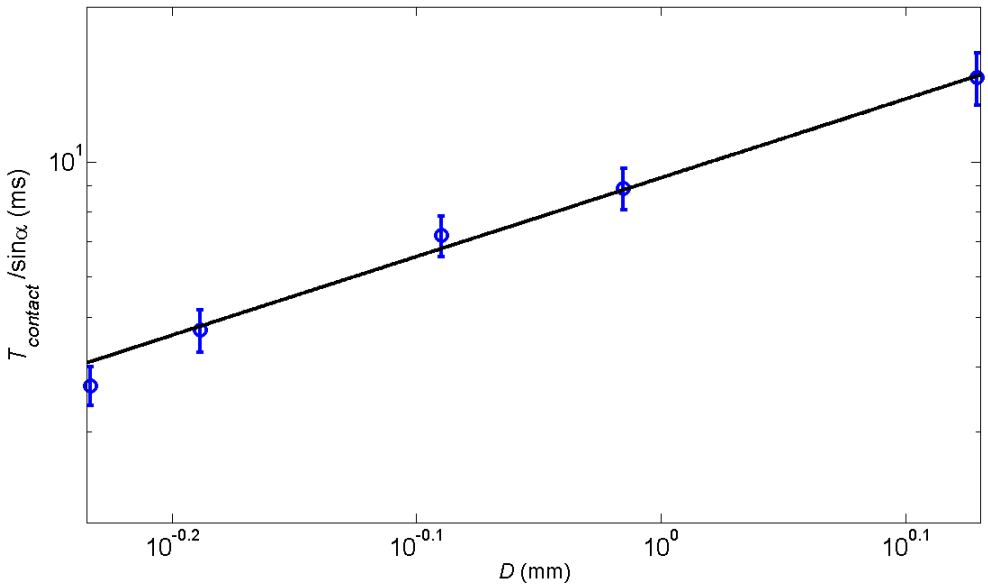

Figure 31: Logarithmic plot between $\frac{T_{contact}}{\sin\alpha}$ and the jet diameter *D*. Straight line is the best fit line on the data with slope = 1.53, 95% confidence bounds = (1.32, 1.74), R^2 = 0.99. Error bar is equal one standard deviation long on each side.

Chapter 5: Conclusions

5.1 Transition from bouncing to coalescence

In the first part of the study, the criteria of transition between bouncing and coalescence in jets are examined. A parametric analysis of the critical jet velocity required for transition from bouncing to coalescence showed that it is dictated by a critical Normal Weber Number $We_{\perp}^{*}$ = 8.23, where $We_{\perp}$ is defined by Equation 1. A critical Weber Number has been found as the criterion of transition in many other non-coalescence studies and thus, the results from this investigation agree with the previous studies [23-27, 32]. This suggests that there is a threshold value for the jet inertia during collision, above which the air-film separating the jets is unable to sustain the forces of collision and gets drained out, leading to coalescence between the jets. It is noted that the characteristic length scale used in the definition of Normal Weber Number $We_{\perp}$ is the thickness of the jets in the vertical direction $\frac{D}{\sin\alpha}$, and only this definition of $We_{\perp}$provides a consistent criterion for the transition. It is not clear why the particular choice of characteristic length scale plays such an important role, and this matter is suggested as a future direction for investigation.

5.2 Contact time of bouncing jets

The second part of the study focuses on the contact time of the jets during the collision. By carrying out the experiment with different jet sizes, angles, velocities and viscosity, a comprehensive picture of the contact time scaling is obtained. Results from the contact time study indicate that the dimensionless contact time scales as the square root of the Normal Weber Number of the colliding jets. This means that the dimensional contact

time of the bouncing jets is independent the velocity of the jets. This result is in good agreement with the previous studies involving drops bouncing on hydrophobic surfaces [21], beads bouncing on elastic membranes [35] and drops bouncing on soap films [32]. The scaling of contact time suggests that during the collision, the surface of the jets acts like a stretched linear spring which absorbs the inertial forces during the impact, and then causes the bounce back of the jets much like the recoil of spring.

5.3 Summary

This thesis is the first attempt towards a detailed parametric study of non-coalescence in fluid jets with the aim of elucidating the role of various physical forces involved in the phenomenon. First, experimental data on the boundary between bouncing and coalescence is required to represent the balance between various antagonist forces involved in the phenomena. Any theoretical model developed to explain the phenomenon of jet bouncing will need to be compared with such experimental observations. Such data is provided in the first subsection of the previous chapter. Secondly, another component of the proposed hypothesis, contact time of the bouncing jets, is examined. Combined together, these components provide important understanding of several aspects of the bouncing jets, but many questions still remain unanswered. These open questions are mentioned in the next sub-section as suggestions for future work.

5.4 Suggestions for future work

Modeling the behavior of air-film, which is imperative to a complete physical understanding of the bouncing jets, remains a challenging problem. Such a model will

allow the estimation of forces that the air-film trapped between the jets is capable of producing, and thus will provide a criterion for coalescence, that can be compared with experimental results presented in Chapter 4. One way to investigate the role played by the surrounding fluid medium is to replace air with other gases with properties different from air, and study the effect it has on the bouncing behavior. The dynamics of sudden coalescence of two jets is another interesting problem which will also provide useful insight to the bouncing behavior. For example, by high speed imaging of the collision region during the coalescence of jets, one can find out the exact location of the start of coalescence. The thickness of trapped air-film is the least at this point in the collision region, so the knowledge of the location of coalescence will shed some light on how the air-film evolves along the collision region.

As mentioned in first section of this chapter, it is not clear why the particular choice of length scales plays a role in deciding the criterion for transition from bouncing to coalescence. The peculiar role played by the geometry of bouncing jets is unique, as the previous studies of non-coalescence of fluid interfaces have usually involved drops, which do not involve the geometrical considerations found in bouncing jets. A more detailed investigation focusing on the geometry effects in scaling arguments will thus be very useful, both for bouncing jets and for understanding of scaling analyses.

In addition, it will be useful to conduct more experiments detailed theoretical and computational studies, which hopefully will complement the understanding gained from experiments.

References

1. Wadhwa, N. and S. Jung, *Non-coalescence of jets.* Physics of Fluids, 2011. **23**(9): p. 091105.
2. Charles, G.E. and S.G. Mason, *The coalescence of liquid drops with flat liquid/liquid interfaces.* Journal of Colloid Science, 1960. **15**(3): p. 236-267.
3. Rayleigh, L., *The influence of electricity on colliding water drops.* Proceedings of the Royal Society of London, 1878. **28**(190-195): p. 405.
4. Rayleigh, L., *Investigations in capillarity.* Philosophical Magazine, 1899. **48**: p. 321.
5. Rayleigh, L., *Further Observations upon Liquid Jets, in Continuation of Those Recorded in the Royal Society's' Proceedings' for March and May, 1879.* Proceedings of the Royal Society of London, 1882. **34**: p. 130-145.
6. Newall, H.F., *IV. On colliding water-jets.* Philosophical Magazine Series 5, 1885. **20**(122): p. 31-34.
7. Boys, C.V., *Soap bubbles, their colours and the forces which mold them*. 1958: Dover Publications.
8. Reynolds, O., *On the floating of drops on the surface of water depending only on the purity of the surface.* Proceedings of the Manchester Literary and Philosophical Society, 1881-82. **21**.
9. Seth, J.B., C. Anand, and L. Das Mahajan, *XXVII. Liquid drops on the same liquid surface.* Philosophical Magazine Series 7, 1929. **7**(42): p. 247-253.
10. Mahajan, L., *Liquid drops on the same liquid surface.* Nature, 1930. **126**(3185): p. 761-761.

11. Mahajan, L.D., *The effect of the surrounding medium on the life of floating drops.* The London, Edinburgh, and Dublin Philosophical Magazine and Journal of Science, 1930. **10**(64): p. 383-386.

12. Sreenivas, K.R., P.K. De, and J.H. Arakeri, *Levitation of a drop over a film flow.* Journal of Fluid Mechanics, 1999. **380**: p. 297-307.

13. Charles, G.E. and S.G. Mason, *The mechanism of partial coalescence of liquid drops at liquid/liquid interfaces.* Journal of Colloid Science, 1960. **15**(2): p. 105-122.

14. Couder, Y., et al., *From Bouncing to Floating: Noncoalescence of Drops on a Fluid Bath.* Physical Review Letters, 2005. **94**(17): p. 177801.

15. Couder, Y., et al., *Dynamical phenomena: Walking and orbiting droplets.* Nature, 2005. **437**(7056): p. 208-208.

16. Protière, S., A. Boudaoud, and Y. Couder, *Particle–wave association on a fluid interface.* Journal of Fluid Mechanics, 2006. **554**: p. 85-108.

17. Protière, S., et al., *The self-organization of capillary wave sources.* Journal of Physics: Condensed Matter, 2005. **17**: p. S3529.

18. Couder, Y. and E. Fort, *Single-Particle Diffraction and Interference at a Macroscopic Scale.* Physical Review Letters, 2006. **97**(15): p. 154101.

19. Thrasher, M., et al., *Bouncing jet: A Newtonian liquid rebounding off a free surface.* Physical Review E, 2007. **76**(5): p. 056319.

20. Thrasher, M., et al., *Bouncing of a jet off a Newtonian liquid surface.* Physics of Fluids, 2007. **19**(9): p. 091110.

21. Richard, D., C. Clanet, and D. Quere, *Surface phenomena: Contact time of a bouncing drop.* Nature, 2002. **417**(6891): p. 811-811.

22. Clanet, C., et al., *Maximal deformation of an impacting drop.* Journal of Fluid Mechanics, 2004. **517**: p. 199-208.

23. Bradley, S.G. and C.D. Stow, *Collisions between Liquid Drops.* Philosophical Transactions of the Royal Society of London. Series A, Mathematical and Physical Sciences, 1978. **287**(1349): p. 635-675.

24. Ashgriz, N. and J.Y. Poo, *Coalescence and separation in binary collisions of liquid drops.* Journal of Fluid Mechanics, 1990. **221**: p. 183-204.

25. Jiang, Y.J., A. Umemura, and C.K. Law, *An experimental investigation on the collision behaviour of hydrocarbon droplets.* Journal of Fluid Mechanics, 1992. **234**: p. 171-190.

26. Orme, M., *Experiments on droplet collisions, bounce, coalescence and disruption.* Progress in Energy and Combustion Science, 1997. **23**(1): p. 65-79.

27. Qian, J. and C.K. Law, *Regimes of coalescence and separation in droplet collision.* Journal of Fluid Mechanics, 1997. **331**: p. 59-80.

28. Ribeiro Jr, C.P. and D. Mewes, *The effect of electrolytes on the critical velocity for bubble coalescence.* Chemical Engineering Journal, 2007. **126**(1): p. 23-33.

29. Courbin, L. and H.A. Stone, *Impact, puncturing, and the self-healing of soap films.* Physics of Fluids, 2006. **18**(9): p. 091105.

30. Taylor, G. and L. Howarth, *The Dynamics of Thin Sheets of Fluid. I. Water Bells.* Proceedings of the Royal Society of London. Series A. Mathematical and Physical Sciences, 1959. **253**(1274): p. 289-295.

31. Taylor, G.I. and D.H. Michael, *On making holes in a sheet of fluid.* Journal of Fluid Mechanics, 1973. **58**(04): p. 625-639.

32. Gilet, T. and J.W.M. Bush, *The fluid trampoline: droplets bouncing on a soap film.* Journal of Fluid Mechanics, 2009. **625**: p. 167-203.

33. Sheely, M.L., *Glycerol Viscosity Tables.* Industrial & Engineering Chemistry, 1932. **24**(9): p. 1060-1064.

34. Weast, R.C., M.J. Astle, and W.H. Beyer, *CRC handbook of chemistry and physics*. Vol. 69. 1988: CRC press Boca Raton, FL.

35. Courbin, L., et al., *Impact Dynamics for Elastic Membranes.* Physical Review Letters, 2006. **97**(24): p. 244301.

Appendix A: MATLAB© code for image analysis

```
% This program takes the jpg format experimental images as input and
% analyzes them digitally to measure the contact length between the
jets
% and the angle of incoming and outgoing jets with the vertical axis.
% Several user checkpoints have been added in the code to ensure that
there
% is no error in the measurements.


clc
clear
TF = 1;
[f,path] = uigetfile('../*.mat','Select calibration
file','C:\Users\Saikat\Desktop\Navish\Research\Summer 2011
Experiemnts');
% Select the calibration file for measurement of distance. used for
% measurement of contact length
cal_file = strcat(path,f);
load(cal_file)
thres = 0.5; %Threshold for grayscale to binary conversion.
% Results are sensitive to this parameter, so I included a checkpoint
to adjust this
pix = 400; % Pixel distance of points for calculation of incoming angle
pix2 = 400; % Pixel distance of points for calculation of outgoing
angle
PathName = path;
Gauge = 18; % Change this when using for a different gauge number
ID = 0.038; % Change this when using for a different gauge number
Count = 0;
Out = {'Flow' 'Contact Length' 'Angle In Right' 'Angle In Left' 'Angle
Out Right' 'Angle Out Left' 'Err_U' 'Err_L' 'File' 'Gauge' 'ID(in)'};
while TF == 1 % flag
    Count = Count+1;
    [FileName,PathName,FilterIndex] =
uigetfile({'*.jpeg';'*.jpg'},'Select image', PathName); % Select image
    cd(PathName)
    file = strcat(PathName,FileName);
    choice = 'No';
    V_vec = [0 -5000]; % Vertical axis pointing upwards
    I1 = imread(file);
    imshow(I1);
    title(file(end-7:end-4));
    H = imrect;
    pos = getPosition(H);
    close
    I1 = imcrop(I1, pos);
    I1 = rgb2gray(I1);

    while strcmp(choice,'No') == 1
        I = im2bw(I1,thres);
        I2 = imcomplement(I);
        dim = size(I);
```

```
        col_u = round(dim(2)/2);
        row_u1 = find(I2(:,col_u), 1)-1;
        row_u2 = find(I2(:,col_u), 1);
        if row_u1 ~= 0
            boundary_u1 = bwtraceboundary(I,[row_u1, col_u],'W');
            boundary_u2 = bwtraceboundary(I2,[row_u2, col_u],'W');
            [y_u1, k1] = max(boundary_u1(:,1));
            [y_u2, k2] = max(boundary_u2(:,1));
            x_u1 = boundary_u1(k1,2);
            x_u2 = boundary_u2(k2,2);

            col_l = x_u1;
            row_l1 = find(I2(:,col_l), 1, 'last')+1;
            row_l2 = find(I2(:,col_l), 1, 'last');
            if row_l1 < dim(1)
                boundary_l1 = bwtraceboundary(I,[row_l1, col_l],'W');
                boundary_l2 = bwtraceboundary(I2,[row_l2, col_l],'W');
                [y_l1, j1] = min(boundary_l1(:,1));
                [y_l2, j2] = min(boundary_l2(:,1));
                x_l1 = boundary_l1(j1,2);
                x_l2 = boundary_l2(j2,2);

                hold off
                imshow(I)
                hold on;

plot(boundary_u1(:,2),boundary_u1(:,1),'g','LineWidth',2);

plot(boundary_l1(:,2),boundary_l1(:,1),'g','LineWidth',2);

plot(boundary_u2(:,2),boundary_u2(:,1),'b','LineWidth',2);

plot(boundary_l2(:,2),boundary_l2(:,1),'b','LineWidth',2);
                title(file(end-7:end-4));

                if col_u < x_u1
                    J_vec1 = [boundary_u1(k1-pix,2)-x_u1
boundary_u1(k1-pix,1)-y_u1];
                    J_vec2 = [boundary_u1(pix,2)-x_u1
boundary_u1(pix,1)-y_u1];
                    plot(boundary_u1(k1-pix,2),boundary_u1(k1-
pix,1),'o','LineWidth',3);

plot(boundary_u1(pix,2),boundary_u1(pix,1),'o','LineWidth',3);
                else
                    J_vec1 = [boundary_u1(end-pix,2)-x_u1
boundary_u1(end-pix,1)-y_u1];
                    J_vec2 = [boundary_u1(k1+pix,2)-x_u1
boundary_u1(k1+pix,1)-y_u1];
                    plot(boundary_u1(end-pix,2),boundary_u1(end-
pix,1),'o','LineWidth',3);

plot(boundary_u1(k1+pix,2),boundary_u1(k1+pix,1),'o','LineWidth',3);
                end

                if col_l > x_l1
```

```
                    K_vec2 = [boundary_l1(j1-pix2,2)-x_l1
boundary_l1(j1-pix2,1)-y_l1];
                    K_vec1 = [boundary_l1(pix2,2)-x_l1
boundary_l1(pix2,1)-y_l1];
                    plot(boundary_l1(j1-pix2,2),boundary_l1(j1-
pix2,1),'o','LineWidth',3);

plot(boundary_l1(pix2,2),boundary_l1(pix2,1),'o','LineWidth',3);
                else
                    K_vec2 = [boundary_l1(end-pix2,2)-x_l1
boundary_l1(end-pix2,1)-y_l1];
                    K_vec1 = [boundary_l1(j1+pix2,2)-x_l1
boundary_l1(j1+pix2,1)-y_l1];
                    plot(boundary_l1(end-pix2,2),boundary_l1(end-
pix2,1),'o','LineWidth',3);

plot(boundary_l1(j1+pix2,2),boundary_l1(j1+pix2,1),'o','LineWidth',3);
                end

                plot(x_u1,y_u1,'ro','LineWidth',3);
                plot(x_l1,y_l1,'ro','LineWidth',3);
                plot(x_u2,y_u2,'ro','LineWidth',3);
                plot(x_l2,y_l2,'ro','LineWidth',3);

                qstring = 'Continue with the current threshold?';
                choice = questdlg(qstring,'Continue?');
                if strcmp(choice,'Cancel')
                    q = 'Skip image?';
                    opt = questdlg(q,'Skip?');
                    if strcmp(opt,'Yes')
                        break
                    end
                end
                if strcmp(choice,'No')
                    prompt = {'Enter new threshold'};
                    dlg_title = 'Input threshold';
                    num_lines = 1;
                    def = {num2str(thres)};
                    answ = inputdlg(prompt,dlg_title,num_lines,def);
                    thres = str2num(answ{1});
                else
                    Flow = str2double(PathName(77:end-1));
                    L = calib*sqrt((0.5*(x_u1+x_u2)-0.5*(x_l1+x_l2))^2
+ (0.5*(y_u1+y_u2)-0.5*(y_l1+y_l2))^2);
                    Ang_Rin = acosd(dot(V_vec,
J_vec1)/(norm(V_vec)*norm(J_vec1)));
                    Ang_Lin = acosd(dot(V_vec,
J_vec2)/(norm(V_vec)*norm(J_vec2)));
                    Ang_Rout = acosd(dot(-V_vec, K_vec1)/(norm(-
V_vec)*norm(K_vec1)));
                    Ang_Lout = acosd(dot(-V_vec, K_vec2)/(norm(-
V_vec)*norm(K_vec2)));
                    err_u = calib*sqrt((x_u2-x_u1)^2 + (y_u2-y_u1)^2);
                    err_l = calib*sqrt((x_l2-x_l1)^2 + (y_l2-y_l1)^2);
                    p = size(Out, 1);
                    Out{p+1,1} = Flow;
                    Out{p+1,2} = L;
```

```
                    Out{p+1,3} = Ang_Rin;
                    Out{p+1,4} = Ang_Lin;
                    Out{p+1,5} = Ang_Rout;
                    Out{p+1,6} = Ang_Lout;
                    Out{p+1,7} = err_u;
                    Out{p+1,8} = err_l;
                    Out{p+1,9} = file(end-7:end-4);
                    Out{p+1,10} = Gauge;
                    Out{p+1,11} = ID;
                end

            else
                prompt = {'Threshold too large or too small, enter new
threshold'};
                dlg_title = 'Input threshold';
                num_lines = 1;
                def = {num2str(thres)};
                answ = inputdlg(prompt,dlg_title,num_lines,def);
                if strcmp(answ,'')
                    q = 'Skip image?';
                    opt = questdlg(q,'Skip?');
                    if strcmp(opt,'Yes')
                        break
                    end
                end
                thres = str2num(answ{1});
            end
        else
            prompt = {'Threshold too large or too small, enter new
threshold'};
            dlg_title = 'Input threshold';
            num_lines = 1;
            def = {num2str(thres)};
            answ = inputdlg(prompt,dlg_title,num_lines,def);
            if strcmp(answ,'')
                q = 'Skip image?';
                opt = questdlg(q,'Skip?');
                if strcmp(opt,'Yes')
                    break
                end
            end
            thres = str2num(answ{1});
        end
    end
    button = questdlg('Another image in this
folder?','Continue?','Yes','No','Yes');
    TF = strcmp(button, 'Yes');
    xlswrite('data.xlsx', Out)
    close(gcf)
%     Flow
end
```